



NLR TP 97665

NLR-TU Delft Experience in Unsteady Aerodynamics and Aeroelastic Simulation Applications

J.J. Meijer, M.H.L. Hounjet, B.J.G. Eussen and B.B. Prananta

DOCUMENT CONTROL SHEET

	ORIGINATOR'S REF.		SECURITY CLASS. TP 97665 U																		
ORIGINATOR National Aerospace Laboratory NLR, Amsterdam, The Netherlands																					
TITLE NLR-TUDeft experience in unsteady aerodynamics and aeroelastic simulation applications																					
PRESENTED AT the RTO Workshop: "Unsteady Aerodynamic Computations and Computational Aeroelastic Simulations", Aalborg, DK, October 14 - 15, 1997																					
AUTHORS J.J. Meijer, M.H.L. Hounjet, B.J.G. Eussen, B.B. Prananta		DATE 971101	<table style="width: 100%; border: none;"> <tr> <td style="text-align: center;">pp</td> <td style="text-align: center;">ref</td> </tr> <tr> <td style="text-align: center;">25</td> <td style="text-align: center;">34</td> </tr> </table>	pp	ref	25	34														
pp	ref																				
25	34																				
DESCRIPTORS <table style="width: 100%; border: none;"> <tr> <td style="width: 33%;">Aerodynamics</td> <td style="width: 33%;">Grid generation (mathematics)</td> <td style="width: 33%;">Numerical analysis</td> </tr> <tr> <td>Aeroelasticity</td> <td>Computerized simulation</td> <td>Unsteady aerodynamic</td> </tr> <tr> <td>Aircraft</td> <td>Delta wings</td> <td>Wing loading</td> </tr> <tr> <td>Aircraft design</td> <td>Fighter aircraft</td> <td>Wing</td> </tr> <tr> <td>Body-wing and tail configurations</td> <td>Flutter</td> <td></td> </tr> <tr> <td>Computational fluid dynamics</td> <td>Mathematical models</td> <td></td> </tr> </table>				Aerodynamics	Grid generation (mathematics)	Numerical analysis	Aeroelasticity	Computerized simulation	Unsteady aerodynamic	Aircraft	Delta wings	Wing loading	Aircraft design	Fighter aircraft	Wing	Body-wing and tail configurations	Flutter		Computational fluid dynamics	Mathematical models	
Aerodynamics	Grid generation (mathematics)	Numerical analysis																			
Aeroelasticity	Computerized simulation	Unsteady aerodynamic																			
Aircraft	Delta wings	Wing loading																			
Aircraft design	Fighter aircraft	Wing																			
Body-wing and tail configurations	Flutter																				
Computational fluid dynamics	Mathematical models																				
ABSTRACT NLR is developing a numerical aeroelastic simulation environment for applications to civil and fighter-type aircraft, of which a pilot version is in cooperation. In addition to extensive validation of the code, special attention has been given to the design of user-friendly pre- and postprocessing. The present paper addresses the motivation of an aeroelastic simulation environment, the status of the NLR AE roelastic SIM ulation system, the current research activities, the pre- en postprocessing and future research activities. Several applications will be shown, demonstrating the use to both civil and fighter-type aircraft. EINDEVELD																					

NLR-TU Delft Experience in Unsteady Aerodynamics and Aeroelastic Simulation Applications

J.J. Meijer **M.H.L. Hounjet** **B.J.G. Eussen**
meijer@nlr.nl hounjet@nlr.nl eussen@nlr.nl
National Aerospace Laboratory, NLR
Amsterdam, The Netherlands

B.B. Prananta
b.b.prananta@lr.tudelft.nl
Delft University of Technology
Delft, The Netherlands

SUMMARY

NLR is developing a numerical aeroelastic simulation environment for applications to civil and fighter-type aircraft, of which a pilot version is in operation. In addition to extensive validation of the code, special attention has been given to the design of user-friendly pre- and postprocessing.

The present paper addresses the motivation of an aeroelastic simulation environment, the status of the NLR **A**Eroelastic **S**IMulation system, the current research activities, the pre- and postprocessing and future research activities. Several applications will be shown, demonstrating the use to both civil and fighter-type aircraft.

ABBREVIATIONS

CUA	Computational Unsteady Aerodynamics
CAS	Computational Aeroelastic Simulations
CFD	Computational Fluid Dynamics
DL	Doublet Lattice Method
EE	Euler Equations
FEM	Finite Element Method
FP	Full Potential
LCO	Limit Cycle Oscillation
MIMO	Multiple Input/Multiple Output
(TL)NS	(Thin Layer) Navier Stokes

1. INTRODUCTION

The development of aerodynamic and aeroelastic simulation codes is steadily making progress. Nevertheless these codes are only modestly being accepted by the end-users in industry in charge of aeroelastic stability and loads analyses.

Various shortcomings of the current codes can be named which cause the hesitation of engineers to use these codes in practice. This hesitation is mainly associated with the large effort required to build up sufficient experience with, and trust in the new method before it can be used for important and often critical design aspects of the aircraft. Another important barrier for large-scale engineering applications is the large effort needed for pre- and postprocessing of the usually complex computer codes.

NLR is developing a numerical aeroelastic simulation environment for applications to civil and fighter-type aircraft, of which a pilot version is in operation. In addition to extensive validation of the code, special attention has been given to the design of user-friendly pre- and postprocessing.

The objective of the present paper is a review of the current status and ongoing research at NLR of

- the technological readiness of both Computational Unsteady Aerodynamics (CUA) and Computational Aeroelastic Simulations (CAS),
- the industrial readiness of these methods in practical applications.

Since the last meeting in this subject area [1, 2, 3] many advances were made at NLR in refining mathematical models, applications to more complex aircraft configurations and computational efficiency.

However, a gradually increasing gap exists between the technological and industrial readiness, manifested e.g. by an overpresentation of contributions in this research area from the side of research institutes and universities in comparison with industry. A preparatory step to diminish this gap was presented in [4], which describes the industrial needs and expectations of CUA/CAS.

The subject here is being addressed because of these industrial needs for an efficient aeroelastic simulation system, which is able to improve aircraft design with adequate and efficient assessment of aeroelastic behaviour (flutter and/or dynamic responses) for transonic flight or other nonlinear conditions.

Today's industrial aeroelastic studies are still performed mainly with a set of classical methods based on linear assumptions, supplemented with correction procedures for real flight conditions and many years of experience. These methods have a large efficiency in assessing the critical state cases for a large state space. However, the limited accuracy of such methods for transonic conditions puts a severe limitation to optimization of the aircraft design. The development of advanced CUA and CAS methods may contribute to improve significantly upon this situation, provided that the codes are well validated and the preprocessing, use and postprocessing are optimized to satisfy the aeroelastic requirements in industry.

The NLR AESIM method is developed with the objective to assist in the design of future aircraft which are subjected to increases in flexibility, aerodynamic loading and nonlinearity and might be of value in the early design and development phase for assessing flight stability and control, safety and risk valuation and ride qualities. The method focuses primarily on aeroelasticity at transonic and mildly separated flow conditions where aerodynamic nonlinearities are a non-negligible factor and the accuracy of conventional methods is the most uncertain.

The system was developed primarily for flutter certification of transport-type aircraft, with the aim to become an affordable tool for industry. Recently activities have been started to extend the AESIM method towards flows and geometries which are relevant for fighter-type aircraft. The resulting code will be ready to prove its value in applications with mild flow separation, which is primarily responsible for inducing strong Limit Cycle Oscillation (LCO) structural responses and which might restrict the flight envelope of the aircraft.

In the next section an outline is presented of the current status and ongoing research activities of the CUA/CAS method AESIM, which will be discussed and illuminated with applications in the subsequent sections.

2. OUTLINE

In order to identify the current status of the AEroelastic SIMulation system and the current research activities a list of the main and sub items have been given below. The aim of these activities are to obtain a realistic and affordable aeroelastic simulation system for both transport- and fighter-type aircraft.

- **Motivation**

- * **Realistic and Affordable aeroelastic simulation**

- **AEroelastic SIMulation system status [5, 6]**

- * **Realism**

- ★ Application of flow solver for off-design conditions
 - ★ Application of aeroelastic simulation beyond the envelope usually demonstrated by design codes
 - Solver downgrading in difficult areas to incompressible flow
 - ★ Aeroelastic Accuracy
 - Arbitrary grid reduction in I-, K-direction

- * **Affordability**

- ★ Tailoring of Surface and Field grid generation
 - ★ Volume Spline Interpolation [7]
 - ★ Efficient flow solvers linear DL, FP, EE, TLNS [8, 9]
 - ★ Efficient aero-structural coupling methods [10]
 - ★ Direct visualization and on-line analysis
 - ★ Analysis from single point towards multi-point prediction [11]
 - ★ No ad-hoc implementations

- **Current research activities**

- * **MIMO research**

- ★ CEAS Rome 1997 paper Hounjet/Eussen/Soijer [11]
 - ★ Cooperation Delft University of Technology
 - ★ Points of attention:
 - Multi-point strategy
 - Signal processing

- * **TLNS+ research**

- ★ CEAS Rome 1997 paper Prananta/Hounjet [10]
 - ★ Cooperation Delft University of Technology
 - ★ Superiority TLNS for LANN wing
 - ★ Points of attention:
 - Time-step reduction/Extrapolation methods
 - Prognostics using TAM
 - Turbulence models

- * **Linear aero research**

- ★ CEAS Rome 1997 paper Hounjet/Eussen/Soijer [11]
 - ★ Points of attention:
 - Complex curve fitting
 - Transfer functions for control system design
 - Most straightforward approach

- * **LCO simulation system [12]–[15]**

- ★ CEAS Rome 1997 paper Meijer [15]
 - ★ LCO database experience

- **Future research activities**

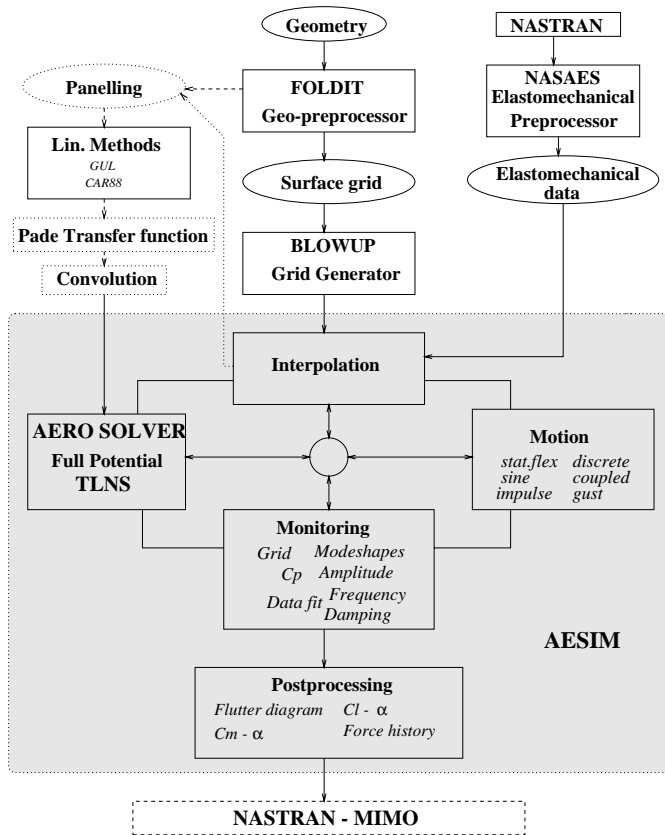


Figure 1: AEroelastic SIMulation system.

3. AEROELASTIC SIMULATION SYSTEM

At NLR much effort has been spent to create a complete AEroelastic SIMulation system, to be used primarily for the flutter certification of transport-type aircraft in the transonic speed regime. Time-accurate simulation of fluid and airframe structure interaction is emphasized. The AEroelastic SIMulation system is referred to as AESIM, after the name of the core program.

The AEroelastic SIMulation system is built around the AESIM core and consists of six independent main program modules, (Fig. 1):

- **FOLDIT**: surface grid generation.
- **BLOWUP**: grid generation.
- **NASAES**: elastomechanical data manipulation.
- **AESIM** core.
- Output interfacing e.g. to NASTRAN or MIMO.
- Linear methods library.

The AESIM core program is divided into 5 individual modules and contains those subroutines which are CPU intensive and make it possible to run the core in stand alone mode:

- **Interpolation**: Interpolation of elastomechanical and aerodynamic data (Volume Spline Method [5, 7]).
- **Aero solver**: Time-accurate solving of aerodynamic equations (FP and TLNS¹).
- **Motion**: Either description of motions, seeded flows, or solving of elastomechanical equations with or without external loadings.

¹Recently the TLNS methodology as reported in [8, 9] has been embedded.

- **Monitoring**: Visualization of simulated data.
- **Postprocessing**: Recollection and assimilation of facts and figures of past simulation(s).

The various aspects of this environment will now be discussed in some detail.

3.1 Surface grid generation

Consistent with aeroelastic requirements and discussed in [5] only the sub-structures of aircraft which are slender and have surfaces with low curvature (wing, tail and fin) need to be modelled quite well in obtaining the aerodynamic force in normal direction. Consequently the quality and density of the surface grids can be relaxed in the other areas. While the aeroelastician is not expected to be an expert surface modeller who creates a surface grid from scratch, the assumption is made that an initial surface grid is available which can be tuned to his needs in routine applications by the geometry pre-processor.

The geometry preprocessor FOLDIT generates a mono-block structured surface description and/or paneling of the complete aircraft with embedded upwind slits and downwind slits (wake surfaces) by assembling and interpolating separate parent surface grids (provided by the user by means of CAD/CAM programs). Instrumental in assisting the user in specifying the required spacing of each component in order to obtain smooth transitions is the so-called **domino** approach. This approach requires the input of the spacings and the number of patches for a few of the parent surface grids which are interpolated (extrapolated) by the volume spline method [7] to the other surface grids. On the floor this means that the user only has to specify the leading and trailing edge resolution of the lifting parts.

FOLDIT also constructs the slits, allows for redistributions, data editing, data smoothing and stripping and tailors the configuration to aeroelastic needs. By this, considerable flexibility is offered to the aeroelastician who is not directed to other programs when minor changes have to be made for parametric studies. Also identification tags are generated which may be required by the interpolation of the elastomechanical data to the surface grid.

3.2 Grid generation

The grid generation is performed by the hyperbolic grid generation method BLOWUP described in [16]. The effort to generate mono-block **HO** grids about the surface description of the complete aircraft with embedded upwind slits and downwind slits (wake surfaces) with mild concavities is low enough to be applied by 'non-grid expert applicators'. The grids have acceptable quality about concave areas such as airfoil noses and wing-fuselage junctions. The consequence of some limitations in accuracy of the mono-block grid approach to more complex configurations is considered acceptable for aeroelastic applications rather than for performance design.

In the solution of the aforementioned modelling, additional in-plane dissipation terms are applied which are

well described in [17]. In addition, metric regularization terms have been developed to guarantee a proper behavior at axis, slit tips, strongly swept surfaces and non-smooth surface grids at wing-body junctions, tip regions, etc.

Also it has turned out that the constant implicitness parameters which are applied nowadays in most hyperbolic grid generators and control the out-of-plane dissipation required for preventing grid lines from crossing in the marching direction should be enhanced to prevent impairing the grid in convex zones. Therefore NLR has introduced a flexible implicitness parameter which can be applied more selective (small in convex zones and large in concave zones) and has worked well in all cases treated so far.

Many configurations can be gridded without angle control terms. In this case one relies on the dissipation terms for rendering concave domains. However, for some cases experiencing very strong concavities it might be necessary to use one of the following angle control options:

- The terms are automatically derived from previously generated planes.
- The terms are built from directions of the far field.
- The terms are evaluated by a 2-D aerodynamic panel method.
- The terms are provided by the surface(volume) spline method.
- The terms are provided from a feedback procedure to prevent grid folding.

In addition BLOWUP has been equipped with the possibilities:

- Starting with an orthogonal grid.
- Post-elliptic smoothing with control functions to smooth the grid. The smoothing is primarily meant for smoothing the transition zone between the hyperbolic and the algebraic generated grid contours and in strong concave zones.
- Algebraic grid generation of grid surfaces in the far field (far front, far rear and far radial surfaces) can be applied when outer boundaries are to be prescribed.
- A hyperbolic shooting method is embedded to generate a grid with a fixed far field boundary distribution.
- Finally existing grids can be refined, enlarged and/or smoothed.

Also **CH,CO** topologies of the grid are provided for single wing applications of the AESIM system. Other topologies that are provided include **HH, XH** and **OC**. A complete description of the BLOWUP grid generator is presented in [18].

3.3 Aerodynamic models

The aeroelastic solver is able to carry out the nonlinear aeroelastic analysis in the subsonic, transonic and supersonic speed range.

At present the time-accurate flow is modelled by:

- FP, completed by the Clebsch potential model for flows with strong shock waves which takes into account entropy and vorticity corrections [19].

The choice for this model, mainly motivated by operational requirements with respect to turn-around time and computational costs, is discussed in [5].

- Recently the EE/TLNS methodology as described in [8, 9] has been embedded because there is enough evidence that with the TLNS complemented with a simple turbulence modelling the needs of the industry can be met for many realistic configurations. The latter extension is motivated by the type of flows and geometries which are encountered with fighter-type aircraft.

3.4 Simulations

The present version of the method enables the following types of simulation around 2-D and 3-D configurations:

- Steady aerodynamic simulation at given M_∞ and angle-of-attack for rigid configuration;
- Steady aeroelastic simulation with static deformations at given M_∞ , angle-of-attack and dynamic pressure;
- Unsteady aerodynamic simulation for forced motion, deformation or gust at given M_∞ , angle-of-attack, vibration mode and type of the motion (gust) (sinusoidal, impulse, jump, polynomial, etc.);
- Unsteady aeroelastic simulation due to elastomechanical motion or deformation at given M_∞ , angle-of-attack, dynamic pressure and vibration modes. Also an external force due to exciters (flutter vane, gusts) can be included.

Simulations can be performed about symmetric configurations with symmetric and/or anti-symmetric vibration modes with respect to the xy (horizontal) and xz (vertical) planes. Also simulations are possible for wing-tail configurations and for complete bodies which require circumferential periodicity conditions to be applied.

On slit surfaces emanating from apices or non-trailing edge body parts the imposing of a hard wall, a free jet or a undisturbed pressure condition can be imposed.

3.5 Elastomechanical model

The elastomechanical model is split into a static part and a dynamic part which are explained in the following sections. The static deformation of the aircraft configuration is obtained by means of the 'free-free' flexibility matrix. The dynamic structural behavior of the aircraft is based on the generalized modal deflection approach. The dynamic deformations are expressed in generalized coordinates q_i and their associated modal mass M , damping D , stiffness K and vibration modes \vec{h}_i . For a description see [5].

3.6 A(ero)E(lasto) Transfer

The information transfer at the fluid/structure interface is performed by the interpolation models which are well described in [7].

From the implemented interpolation models [5] it has turned out in applications that the Least Squares Polynomial approximation of the data and Hounjet's volume spline interpolation method are attractive to select because they do not require any user preparation or intervention. The well-known planar surface spline

interpolation and its curvilinear application are hardly used in applications.

In general it is assumed that the elastomechanical data are obtained through e.g. NASTRAN so that for this case the interface NASAES has been created.

3.7 Others

Besides the vibration modes, other sets of geometric disturbance fields (control modes, pseudo vibration modes) which are interpolated by the volume spline or polynomial spline method might be specified by the user. These modes are also described in [5].

In order to facilitate the comparison with other reference pressure data during the simulation, the volume spline method is also used to interpolate arbitrary data to the aerodynamic surface grid.

3.8 Time signal analysis

One of the fundamental tasks in an aeroelastic analysis is the determination of the frequency and damping of aeroelastic modes (e.g. to detect if one of the generalized displacements becomes unstable and flutter will occur). As many different time response signals may have to be analyzed several methods for curve-fitting should be available. In general each time response signal exists of contributions of various modal modes, of which the frequency and damping of each one have to be determined.

Therefore, during an unsteady simulation the data must be analyzed on-line in the time domain in order to determine the behavior of a coupled system. The main purpose of this analysis is to determine the frequency and damping characteristics of the discrete time signal. To fulfil that task the following methods have been embedded [11]:

- The exponential sine fit,
- Prony's method,
- Fast Fourier Transform analysis,
- Curve-fitting of transfer functions.

Since a wide array of time response signals is available several ways exist to make use of the above-mentioned time-fitting tools. The most common time response signals which can be used to determine the frequency and damping characteristics of the discrete time signal consist of:

- For every modal mode separately:
 - the generalized coordinate,
 - the velocity of the generalized coordinate,
 - the generalized force.
- Also a combination of modal modes and/or the pressure or deformation data at selected points can be analyzed.

3.9 Monitoring and Postprocessing

Direct monitoring and analysis of all aeroelastic quantities of interest are of major importance to the user. The monitoring of the system is able to provide a graphical presentation of the deformations and pressure distribution on the configuration at selected time samples as well as the mean steady pressure distribution and its

first harmonics over a selected time interval. Furthermore, the monitoring is able to provide the dynamic response of integrated loads as lift and moment coefficients for complete configurations as well as individual components. Also the pressure coefficients might be compared with:

- Pressure coefficients generated at a different time or iteration index which is important for checking convergence.
- Pressure coefficients generated in a different session which is important for checking different modellings (e.g. FP against EE).
- Arbitrary reference pressure (experimental) coefficients during the simulation which is important for identification. The volume spline method is used to interpolate the arbitrary data to the aerodynamic surface grid.

When the aeroelastic equations are solved for several flow conditions (variable Mach numbers, angles-of-attack, amplitudes and frequencies of oscillation) facilities are available to monitor and predict the derivatives of the unsteady airloads in that range and to estimate the critical flutter speed.

Attention has been paid to provide the user with 2-D and 3-D plot and analysis facilities to inspect and analyze all aeroelastic quantities of interest during the simulation. At any time the user may interrupt the program for the analyses and inspection of the data. Again this strongly reduces the workload of the aeroelastician who is not directed to other programs for visualization. The visual output includes screen output and off-plot PostScript output.

Except for the mean and first harmonic components of the aforementioned data which is only available after finishing a complete period of a harmonic motion, the data may be required by the user at any time or iteration step.

3.10 Inspection: Screen and PostScript plots

Two kinds of visualization tools are available:

- A 2-D facility for plotting collections of 2-D abscissa-ordinate plots gathered on one screen or on multiple screens.
- A 3-D facility for plotting collections of 3-D surfaces with contour plots and/or vector plots on one screen or on multiple screens.

The facilities may be used to plot the aforementioned quantities depending on the type of simulation. The plots can be stored in color PostScript format (using the special options in the interactive plot facility or using screen dump techniques in combination with other plot facilities.

3.11 Applications

The applicability of the method is directed to 2-D airfoils, 3-D wings, 3-D wing-bodies, T-tail, etc. Many applications of the simulation method were already presented in references [5, 6, 19]. The examples here will focus on current ongoing activities in 3-D to demonstrate the status of the aeroelastic environment. Two applications will be considered. The first one deals with

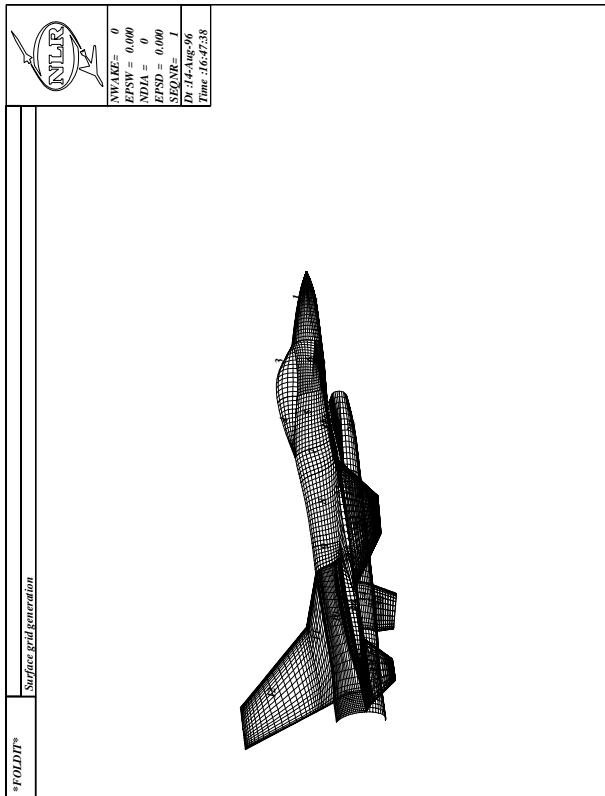


Figure 2: Fighter-type aircraft geometry input for FOLDIT.

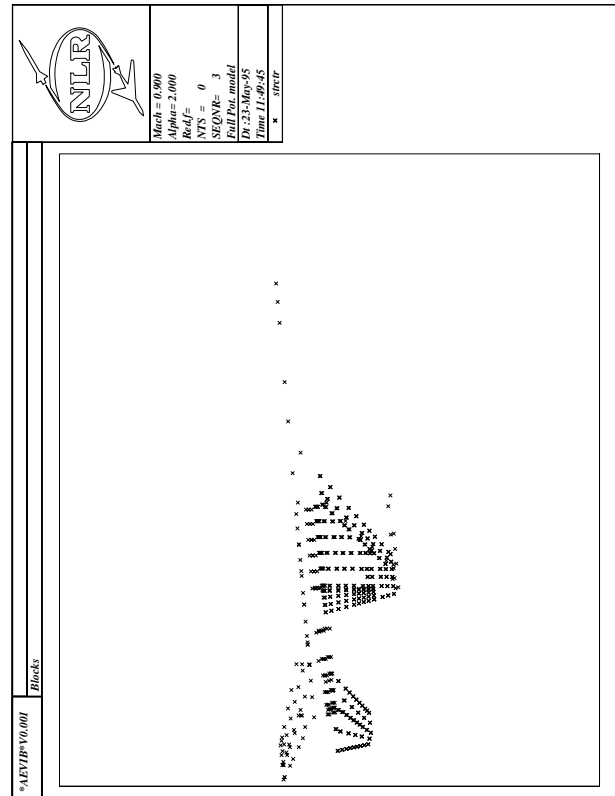


Figure 4: Location of structural points of a fighter-type aircraft.

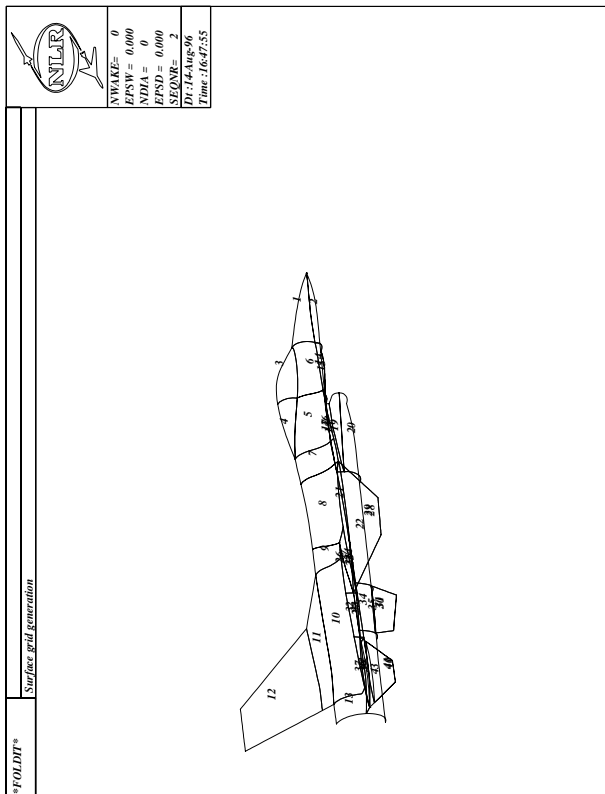


Figure 3: Outline of support surfaces of a fighter-type aircraft.

a fighter-type configuration and the second one with a transport-type T-tail fuselage configuration.

3.11.1 Fighter-type aircraft

In view of the development of time-accurate aerodynamic solvers the ability of the aeroelastic simulation system to deal with fighter-type aircraft (Figs. 2,3) is considered. The complete geometry from ICFM-CFD was processed by **FOLDIT**, in order to obtain a surface grid. The surface grid initiates then the volume grid (Fig. 8). The surface grid should fulfil the requirements to investigate the requested aeroelastic phenomena. This means that tailoring of surface and field grid generation may play an important role.

Running the process to manipulate or tailor the geometry the volume spline interpolation technique [7] has shown to be of invaluable value. This interpolation technique, which may be applied for both structured and unstructured data in general, is demonstrated here for the elastomechanical data transfer between the structural grid and the aerodynamic surface grid.

A NASTRAN finite element model is available from which the symmetric vibration modes and structural grid for a typical fighter-type configuration of the considered aircraft were obtained. In total 679 structural points were applied (Fig. 4). An existing surface grid containing 43 support surface patches (Fig. 3) was used to perform the interpolation.

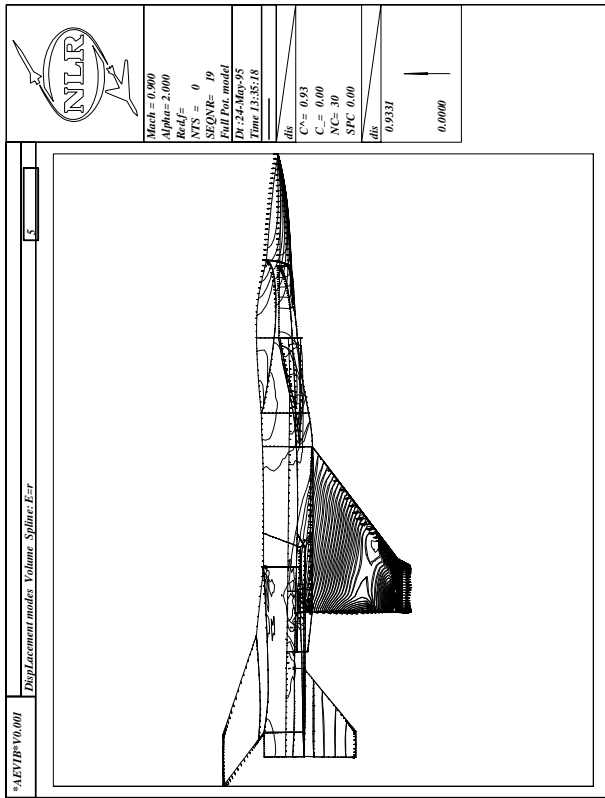


Figure 5: 3-D view of vector plot and contour plot of normal displacements of an arbitrary symmetric vibration mode of a fighter-type aircraft.

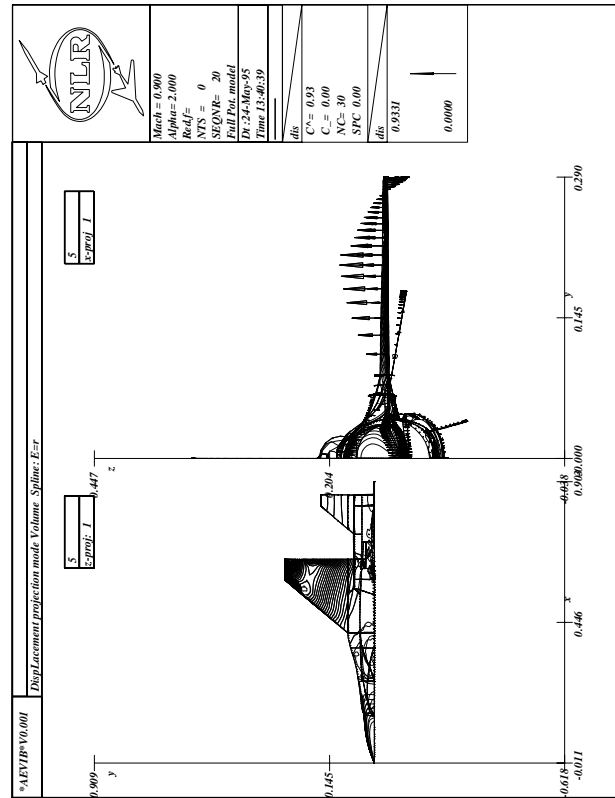


Figure 6: 3-D projections of vector plot and contour plot of normal displacements of an arbitrary symmetric vibration mode of a fighter-type aircraft.

Results are shown in figures 5,6 of an arbitrary symmetric vibration mode (5th). The figures show the outlines of the patches, the displacement vectors at the outlines and contour values of the absolute displacement vector normal to the surfaces. The result of the same symmetric vibration mode obtained with the “standard chain” of computational flutter tools has also been presented in figure 7, which was calculated with a 2-D surface spline technique. It appears that the results shown in figures 5,6 agree well with the result represented in figure 7. Interpolations for other vibration modes demonstrate comparable results as well. More details of interpolation applications are discussed in [7].

Recently the TLNS methodology has been embedded as mentioned in section 3.3. The applicability of the time-accurate TLNS method is demonstrated by comparing calculated data with experimental data for a realistic fighter-type configuration oscillating in pitch at 56.8 % of the root chord with an amplitude of 0.5 deg. The case considered is a transonic flow condition at $M_\infty = 0.92$ and $\alpha_{mean} = 6.0\text{deg}$. The reduced frequency $k = 0.16$ based on the semi-mean aerodynamic chord corresponding with a frequency of $f = 4.5\text{Hz}$ for the real aircraft. Because the robustness of the code for small and large time steps will be shown, only EE results are considered, since from accuracy reasons these allow the largest time steps to be taken. Experimental data are obtained from [3, 20].

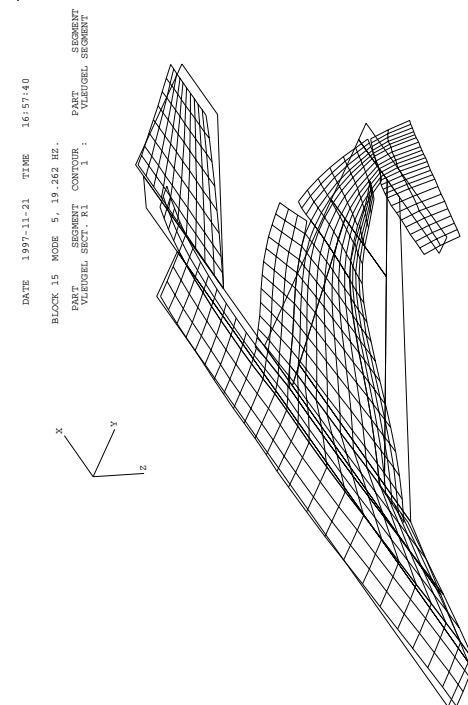


Figure 7: Normal displacements of an arbitrary symmetric vibration mode (5th) of a fighter-type aircraft, from flutter computational chain (surface-spline).

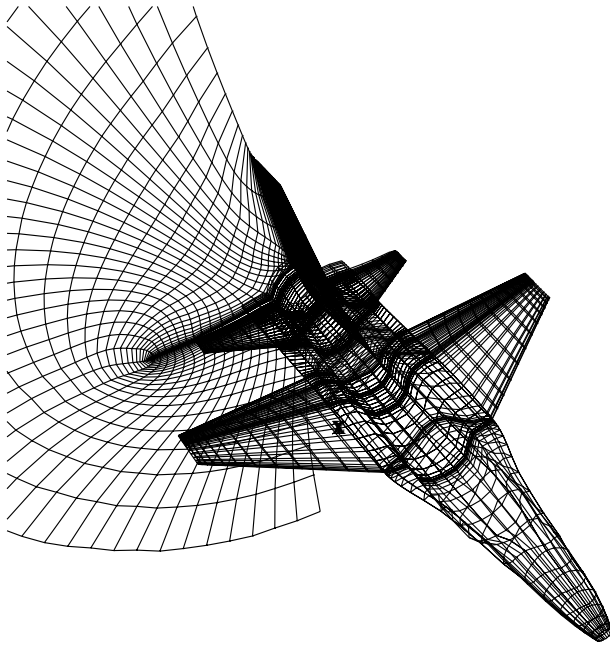


Figure 8: Mesh around wing-body-tail fighter-type configuration, number of points $\sim 200,000$.

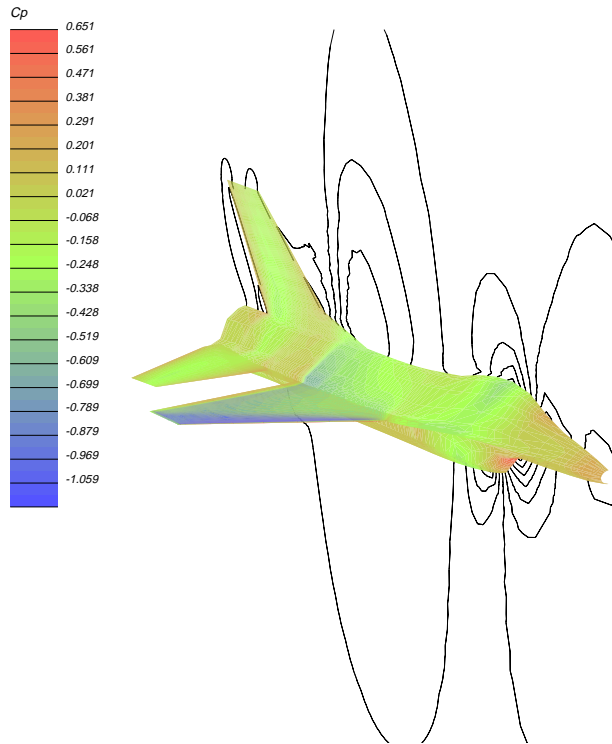


Figure 9: Mean pressure contours (EE) on fighter-type configuration at $M_\infty = 0.92$, $\alpha_m = 6.0$ deg.

Figure 8 shows a mesh with about 200,000 points around the configuration. The inlet of the engine has been smoothed. All results were obtained using FP (fine and coarse grid) and EE equations. Figure 9 shows the mean pressure contours (EE) on the surface of the aircraft. The comparison of the pressure on the upper surface of the wing between the present results (EE,FP)

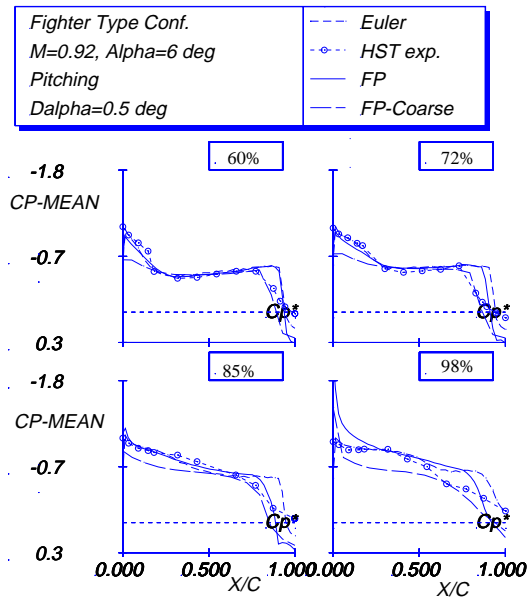


Figure 10: Comparison of experimental and calculated mean pressure distributions on the wing of fighter-type configuration at $M_\infty = 0.92$, $\alpha_m = 6.0$ deg.

and the experimental data is presented in figure 10. The overall agreement is good except at the shock and tip region. The latter may be explained by the fact that the experimental result was obtained using a wind tunnel model having a tip-launcher, while the present calculation was carried out without one. The shock which is too strong may be improved by using the NS equations. Note that the FP calculations both on a fine and on a coarse grid show fairly well results, especially those on the coarse grid perform well except near the tip span station.

Figures 11,12 show the real and imaginary part of the first harmonic pressures (EE,FP) on the upper surface of the wing compared to the experimental results. Two runs were made for the EE calculations employing small time steps (64/cycle) and large time steps (8/cycle). Except for peak values the small time step results as well as the large time step results show a good agreement with the experimental data. Details of the EE calculations are further discussed in [10].

Again the FP calculations both on a fine and on a coarse grid present fairly well results, except for the peak values. In general it can be concluded that the coarse grid does not have sufficient resolution for a detailed description of the unsteady flow, but if one is only interested in a global impression of the flow field and an estimate of hysteresis effects then a coarse grid can be sufficient for a first impression.

3.11.2 T-tail-fuselage

In order to demonstrate the ability of the system to deal with existing aircraft structures the transport-type T-tail fuselage configuration has been chosen (Fig. 13), as discusses in [6]. It should be noted that no parts of the geometry were omitted. The complete geometry from

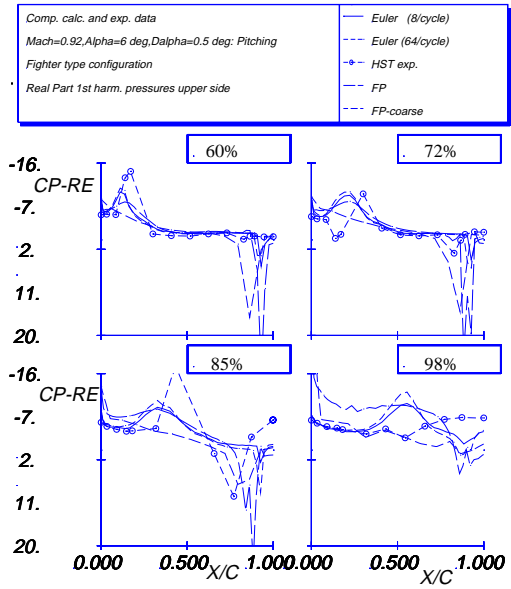


Figure 11: Comparison of experimental and calculated first harmonic pressure distributions (real part) on the wing of fighter-type configuration at $M_\infty = 0.92$, $\alpha_m = 6.0$ deg, $\alpha_{amp} = 0.5$ deg and $k = 0.16$.

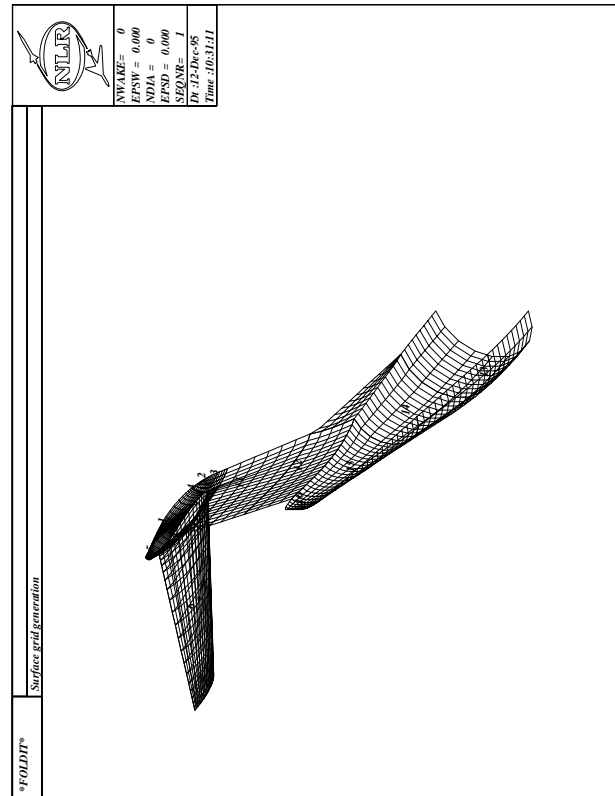


Figure 13: T-tail configuration.

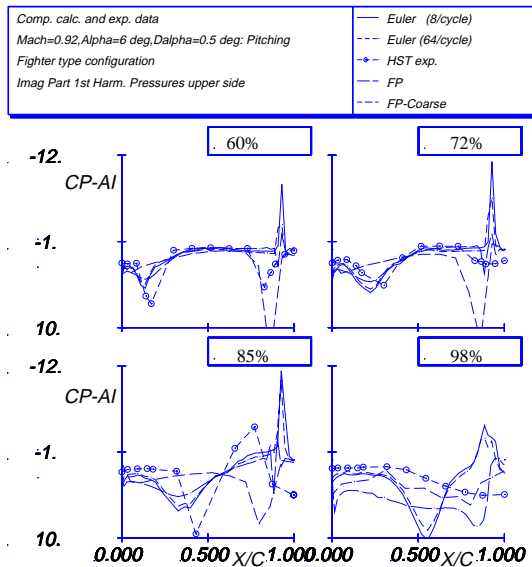


Figure 12: Comparison of experimental and calculated first harmonic pressure distributions (imag. part) on the wing of fighter-type configuration at $M_\infty = 0.92$, $\alpha_m = 6.0$ deg, $\alpha_{amp} = 0.5$ deg and $k = 0.16$.

ICEM-CFD was processed by FOLDIT, in order to obtain a surface grid. The surface grid initiates the volume grid of which characteristic grid planes are shown in reference [6], which shows also the ability of the grid generator to deal with strongly swept wings and non-uniform distributions. For the grid 67x30x33 nodes were applied. Figure 14

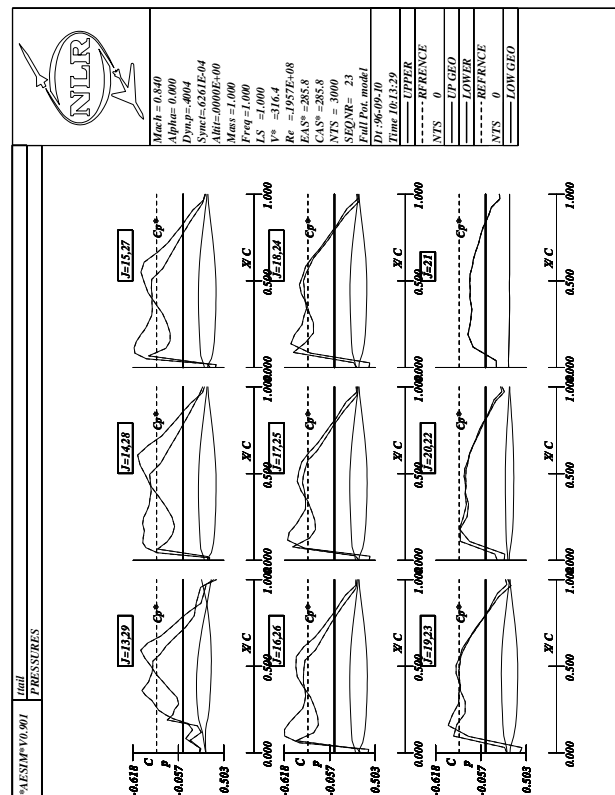


Figure 14: Steady pressure distribution (FP) on horizontal tail.

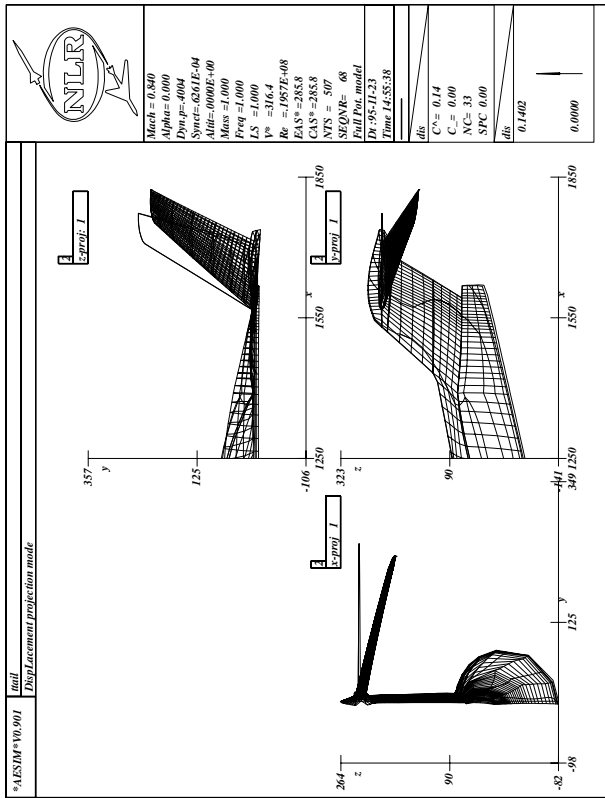


Figure 15: Second mode shape of T-tail configuration.

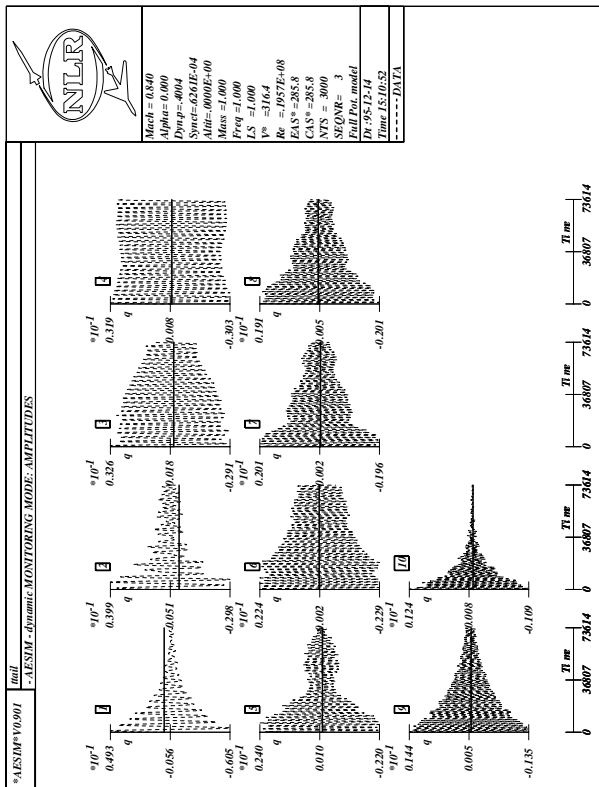


Figure 16: Result of a T-tail configuration of dynamic response of generalized coordinates at $M_\infty = 0.84$ and altitude 0.0 ft in Standard Atmosphere.

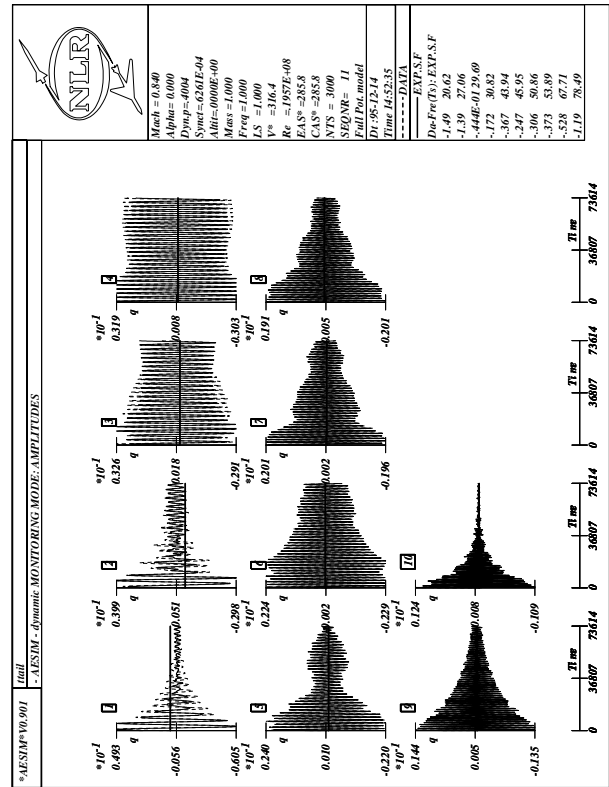


Figure 17: Result of a T-tail configuration after exponential sine fit signal processing of dynamic response of generalized coordinates at $M_\infty = 0.84$ and altitude 0.0 ft in SA.

shows the steady pressure distribution (FP, $M_\infty = 0.84$) on the horizontal tail. From top left to bottom right pressure distributions at different spanwise stations from root to tip are depicted. A considerable transonic flow effect is apparent.

As an example the second mode shape of the T-tail configuration is shown in figure 15. Unsteady calculations (FP aerodynamics) were performed at $M_\infty = 0.84$ and zero altitude in Standard Atmosphere. The elastomechanical model consisted of the first ten vibration modes, obtained with MSC/NASTRAN FEM method. The generalized coordinates of each individual mode were calculated in time as a result of a non-zero initial value for the acceleration of the generalized coordinate. The result of the simulation is shown in figure 16. In figure 17 the time response data is evaluated through exponential sine fit signal processing [11] to get damping and frequency information. The exponential sine fit results compare well with the simulated data. The results of these simulations confirm that the T-tail has a stable dynamic behavior for the flight condition under consideration. This is in accordance with the MSC/NASTRAN flutter diagram [6].

4. CURRENT RESEARCH ACTIVITIES

In this section a number of current research activities are discussed, viz. the subjects:

- MIMO class research
- TLNS+ research

- Linear aero research
- LCO simulation system

4.1 MIMO research

To analyze the many time response signals a number of methods have been embedded (see section 3.8). Very recently a feasibility study has been started to apply

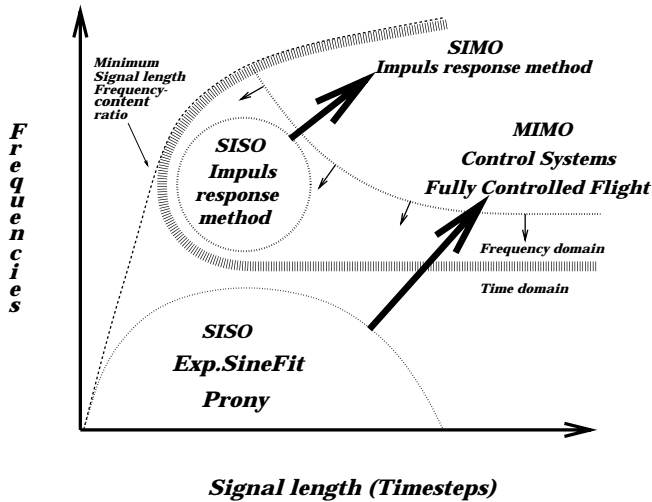


Figure 18: Deployment time-analysis methods with respect to aeroelastic systems.

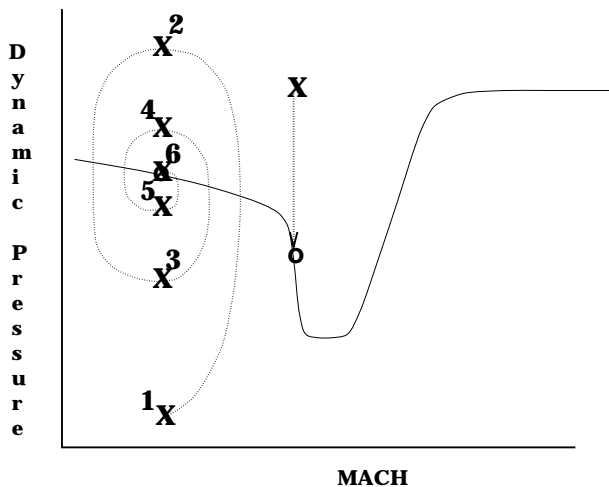


Figure 19: Multi-point strategy.

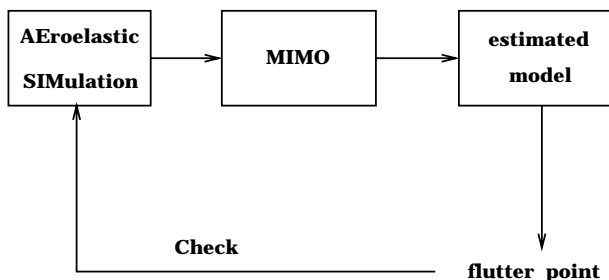


Figure 20: Flowdiagram multi-point strategy.

the promising MIMO-class techniques [21] for that purpose too. They will enhance the analysis capability as depicted in figure 18.

Experience has learned that for a fail safe analysis of an elasto-mechanical system the mentioned fitting routines are applied first to the non-aerodynamically loaded system and next to the system loaded using linear aerodynamics [22], through convolution of transfer functions, [23]. The data from these analyses might act as a guideline for the analysis of the non-linear time signal, originating from the coupled non-linear fluid structure simulation. The analysis process has been fully automated through use of scripts. This facility allows the analysis process to be repeatable and to be documented.

It should be noted that also the analysis might provide a prognostic way to speed up the simulation by allowing for larger time steps [10].

The adoption of MIMO technology [21] permits a black box² evaluation of the aeroelastic system in such a way that after a single fully-coupled simulation for one flight condition the system state for other flight conditions (e.g. q_{dyn}) might be predicted and to extract useful data (e.g. Generalized Forces) from the coupled simulation which can be used for other purposes.

The main purpose is to extend the single point application of coupled simulation methods to multiple points and way-ahead is given to perform postprocessing activities, pk-, k-method etc, with extracted data from an application of a fully-coupled simulation. This multi-point strategy is explained in the figures 19,20 and further described in [21]. A slightly different model structure MIMO* includes auto regressive terms on the outputs. Two examples here focus on current ongoing MIMO activities [11] with respect to the time-analysis and demonstrate the status of the aeroelastic environment too.

4.1.1 AGARD I-wing 445.6

The first example of the applicability of the MIMO-class techniques, in this case the modified MIMO* method, in flutter analysis is presented for an aeroelastic investigation which was conducted for one of the 3-D AGARD standard aeroelastic configurations in subsonic, transonic and supersonic flow. This configuration is described in [24]. The configuration for dynamic response I-wing 445.6 model “weakened no. 3” was selected at Mach=0.901. The data were obtained from [10].

The data (generalized forces) as obtained from simulation with the identified MIMO* model, together with the original data for subcritical flight condition are presented in figure 21. The data has been plotted for time points after the transition has damped out. An excellent agreement is shown between both data sets (they coincide entirely!).

The main purpose of the exercise will be a simulation, at an increased airspeed to a supercritical value, applying the MIMO* results obtained from the subcritical condition and make the comparison with results of the aeroelastic simulation at the higher airspeed. Figure 22

²No knowledge is assumed of coefficients of the structural and aerodynamic system.

depicts the comparison which shows that the system at the supercritical airspeed is unstable and that the linear MIMO* model prediction performs very well for the lower 3 modes. Mode 4 is overpredicted.

Slightly larger errors were found with the MIMO model, i.e. without the auto regressive terms [11]. Which model set results in the best estimates for aerodynamic modelling in aeroelastical closed-loop systems is yet to be investigated.

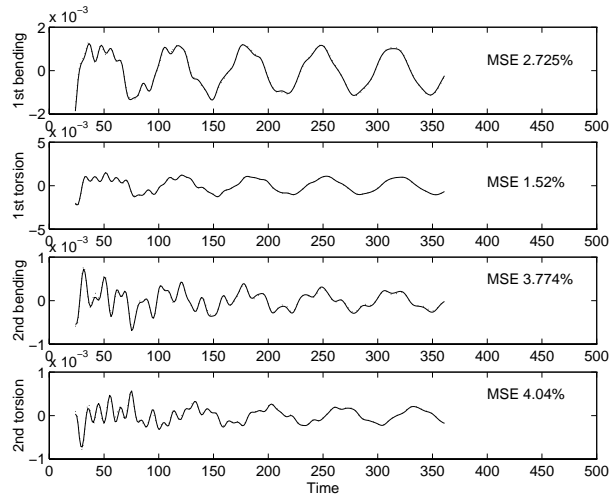


Figure 21: Comparison of MIMO* fitted (...) with auto regressive terms on outputs and original (-) generalized forces data for AGARD I-wing 445.6 at subcritical flight condition.

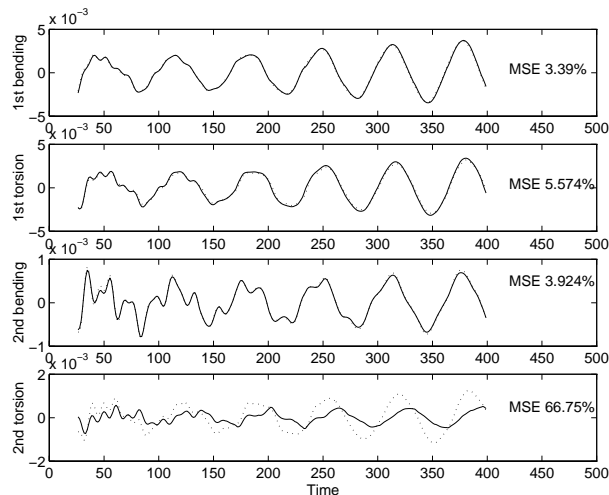


Figure 22: Comparison of MIMO* predicted (...) and reference (-) generalized forces data for AGARD I-wing 445.6 at supercritical flight condition.

4.1.2 T-tail-fuselage

The second example to demonstrate the ability of the MIMO-class techniques deals with the transport-type T-tail fuselage combination, which was already considered in section 3.11.2. The conclusion was that the

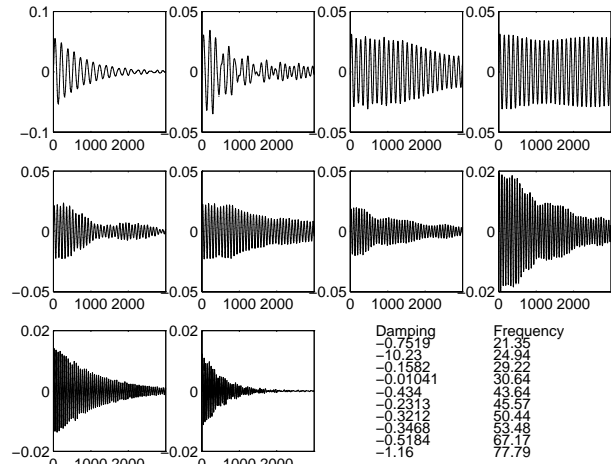


Figure 23: Result of T-tail configuration after MIMO signal processing of dynamic response of generalized coordinates at $M_\infty = 0.84$ and altitude 0.0 ft in SA.

exponential sine fit results (Fig. 17) of the time signals compare reasonably well with the simulated data (Fig. 16). Results with the MIMO-class procedure are depicted in figure 23. The MIMO-class fit results are astonishingly good. Both methods revealed about the same damping and frequencies. The results of these simulations show again that the T-tail has a stable dynamic behavior for the flight condition under consideration.

4.2 TLNS+ research

Transonic aeroelastic investigations of modern aircraft put increasingly higher demands on the accuracy of predicting unsteady aerodynamic loads and aeroelastic characteristics. Methods for numerical aeroelastic simulations have joined, in which the aerodynamics and structural dynamics are considered simultaneously and so provide an integrated approach for the multidisciplinary aeroelastic problems. A central question is the affordability of these methods at various levels of practical applications. It is evident that opinions about affordability depend on local needs conditions and appreciations. It is also clear, however, that answering this question should be based on a thorough insight into potential gains in efficiency and robustness of these methods. The exploration of these gains is a research topic in which Delft university of Technology (DUT) and the National Aerospace Laboratory (NLR) in Amsterdam cooperate.

The outcome of that research so far has been presented in [8, 9, 10] for 2-D and 3-D CUA and CAS methods using EE and TLNS solvers. One of the main features of these solvers is the development of a robust efficient upwind implicit time-marching algorithm for time-accurate TLNS equations, employing subiterations, especially directed to the aeroelastic analysis in viscous transonic flow. The purpose of using subiterations is to accelerate steady-state convergence and to permit a large time step in time-accurate simulations, thereby reducing the computational cost, while maintaining adequate accuracy. Further details are discussed

in [8, 9]. The ability of the method was demonstrated for many cases, including cases of inherently unsteady flow due to shock-induced separation. Considered 3-D cases were: 1) ONERA M6 wing, 2) Fighter-type wings and 3) LANN wing.

Important observations related to practical aeroelastic simulations concluded in [9] were:

- Accurate results have been generated applying not more than 24 and 48 time steps per period for the EE and the TLNS applications, respectively. In that perspective again attention is devoted to the calculation results with EE equations employing small time steps (64/cycle) and large time steps (8/cycle) for a fighter-type configuration (see section 3.11.1 and [9]).
- The methods turned out to be very robust and the only principal user-supplied numerical parameter for an unsteady calculation is the time step.
- The comparison with experiments demonstrated the superiority of the TLNS method over the inviscid methods for cases involving thick wings.
- The 3-D methods have turned out to be about a factor $\mathcal{O}(5)$ to $\mathcal{O}(15)$ slower as compared to a time-accurate FP method for the inviscid and the TLNS applications, respectively. This makes them affordable for embedding in an aeroelastic simulation environment.
- *Since the stability restriction to the time step of the components of the aeroelastic simulation have been strongly relaxed, the next goal is to improve the coupling of the aerodynamic and structural equations.*
- Also it seems to be appropriate now to improve on the turbulence modelling.

Related to the above-mentioned observations a number of current research subjects and/or subjects, which need continuously attention, are discussed and illuminated with some applications. These subjects are:

- Applications of the current TLNS method
- Time-step reduction in CUA applications
- Time-step reduction in CAS applications by:
 - Higher order extrapolation methods
 - Prognostics using Time Analysis Methods (TAM)
- Turbulence models:
 - Baldwin-Lomax
 - Spalart-Allmaras

4.2.1 Semi-span straked delta wing

To investigate the efficiency and robustness of the current TLNS code the applicability is further demonstrated by comparing calculated data with experimental data of the NLR wind tunnel test described in [25] for the semi-span straked delta wing. The geometry of the outer wing panel is the same as that of the fighter-type configuration discussed in section 3.11.1. The flow condition is $M_\infty = 0.90$, $\alpha_m = 6.0$ deg. Steady calculations have been performed with the EE mode of the TLNS code [9] on a mesh of $97 \times 125 \times 30$ grid points.

Figure 24 shows the planform and steady isobar contours at the upper side of the wing with total pressure contours behind the wing. Clearly visible are the vortices initiated by the simple strake and the tip of the outer wing panel. Measured mean pressure contours at the same flow conditions are presented in figure 25.

A qualitative comparison of the pressure contours (Figs. 24,25) on the upper surface at the indicated wing stations of the outer wing panel shows a fairly well agreement, in particular the presence of the lambda shock waves near the tip ³.

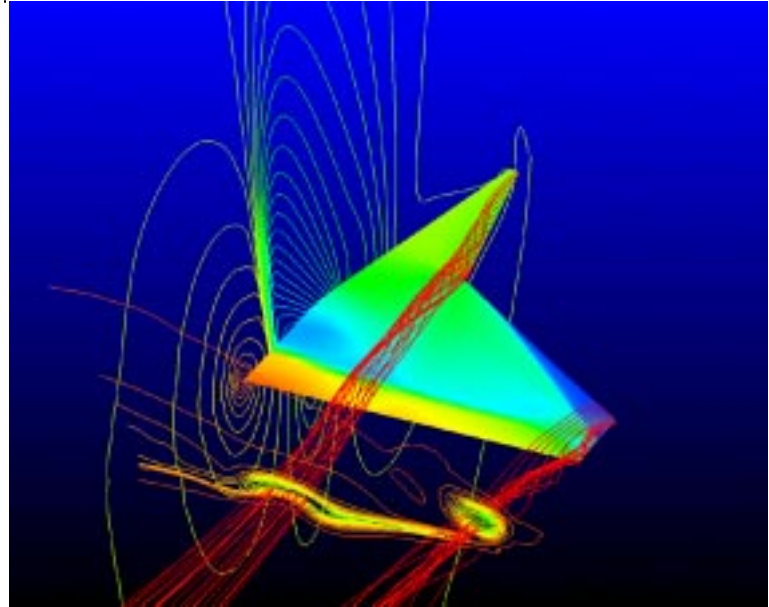


Figure 24: Steady pressure contours (EE) on a semi-span straked delta wing configuration with total pressure contours behind the wing at $M_\infty = 0.90$, $\alpha_m = 6.0$ deg.

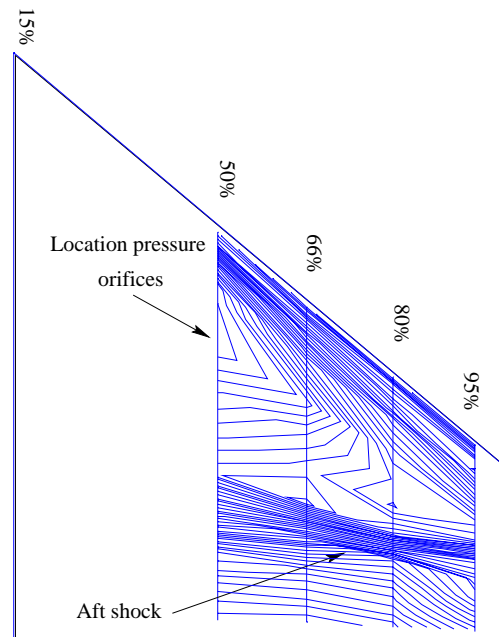


Figure 25: Measured mean pressure contours on a semi-span straked delta wing configuration at $M_\infty = 0.90$, $\alpha_m = 6.0$ deg.

³Quantitative comparisons and results for oscillating conditions in pitch will be presented in a forthcoming publication.

4.2.2 LANN wing

To verify the current TLNS method for 3-D steady and unsteady applications with moderate viscous and transonic effects for cases involving thick wings the LANN wing was selected in [9]. The superiority of the TLNS method over the inviscid methods for the LANN wing was clearly demonstrated. Because of the superiority of the TLNS method and future applications for fighter-type aircraft the results are presented again.

The geometry of the wing has been taken from [26]. The experimental data is obtained from [27]. Extensive comparison of calculated FP data with experimental data was already performed in [28].

Calculations and comparisons were made for pitching oscillation about 62.1% root chord at $M_{infly} = 0.822$, $\alpha_m = 0.6$ deg and $Re_\infty = 7.3 \times 10^6$ based on root chord. The amplitude of oscillation was 0.25 deg, with a reduced frequency $k = 0.102$ based on root semi-chord. The dimension of the grid was $128 \times 32 \times 24$ for the inviscid case and $128 \times 32 \times 36$ for the viscous case. The same surface grid was used in both cases. For the turbulence modelling the simple Baldwin-Lomax algebraic model was applied.

Comparison of the mean pressure distributions is shown in figure 26 at selected span stations. The Euler results show already a substantial offset to the experimental data, even at the lower side. The TLNS data are in fairly good agreement with the experimental data for

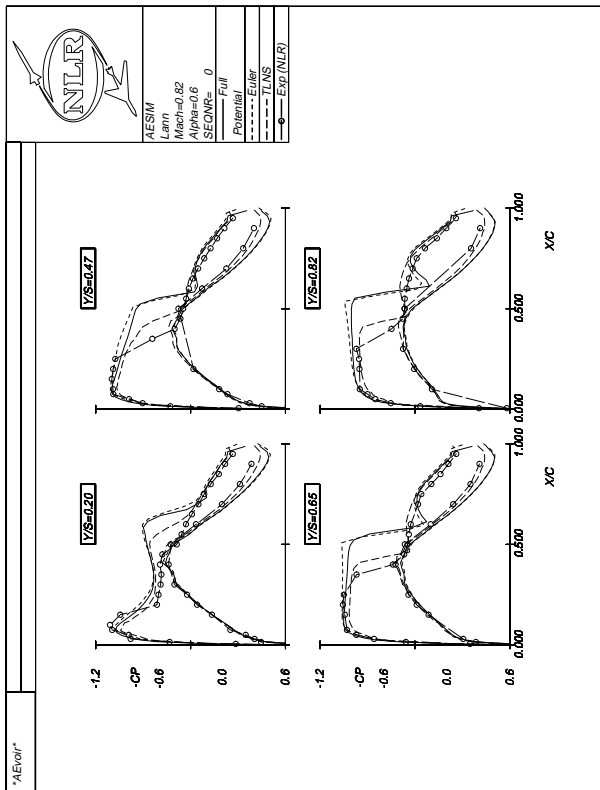


Figure 26: Comparison of experimental with FP, EE and TLNS calculated mean pressure coefficients on LANN transport-type wing, $M_\infty = 0.82$, $\alpha_m = 0.6$ deg and $Re_\infty = 7.3 \times 10^6$.

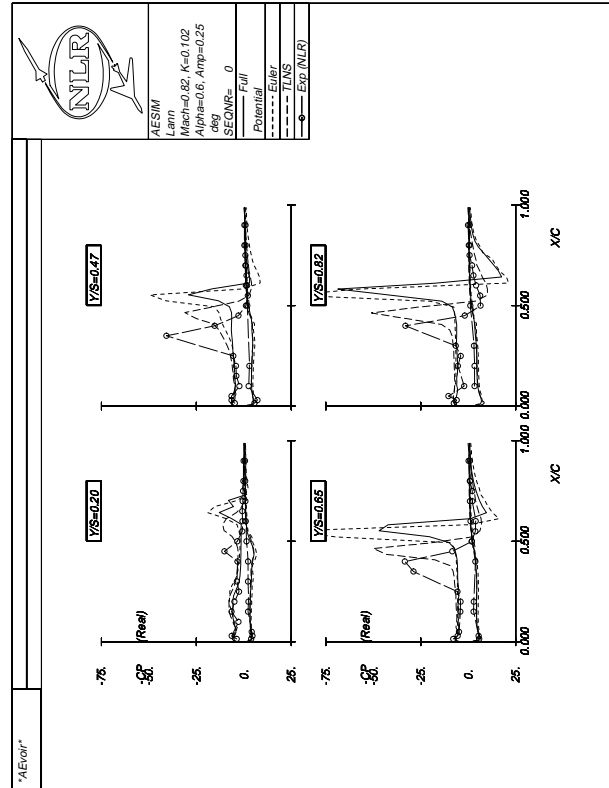


Figure 27: Comparison of real part of experimental with FP, EE and TLNS calculated first-harmonic pressure coefficients on LANN wing at $M_\infty = 0.82$, $\alpha_m = 0.6$ deg, $\alpha_{amp} = 0.25$ deg and $k = 0.102$.

the whole wing at both sides for both shock positions and peak suction levels at the leading edge. Note that the FP results approximate good the Euler data.

Unsteady first harmonic pressure coefficients are compared in figures 27, 28. The EE results were generated with 24(12) time steps per cycle and TLNS results were obtained using 48(16) time steps per cycle.

The lower side shows, except at the root, a subsonic distribution. The upper side shows clearly the effect of the lambda shock waves. Except for peak values the real part of the data is predicted fairly well by the TLNS method. The Euler data show too much differences.

The agreement for the imaginary part of the data is less adequate at both sides. Aft of the shock wave the TLNS method performs better. In front of the shock wave the Euler data seem to compare better.

In general, it has to be concluded that a fairly good agreement has been achieved. Part of the differences between calculated and experimental data should be attributed to the deformation of the wind tunnel model during wind-on conditions and the added complication of peak measurements and integration in the experiment.

4.2.3 Time-step reduction in CUA

In view of the development of a robust and an efficient algorithm for time-accurate TLNS equations to obtain a realistic and affordable simulation system an earlier

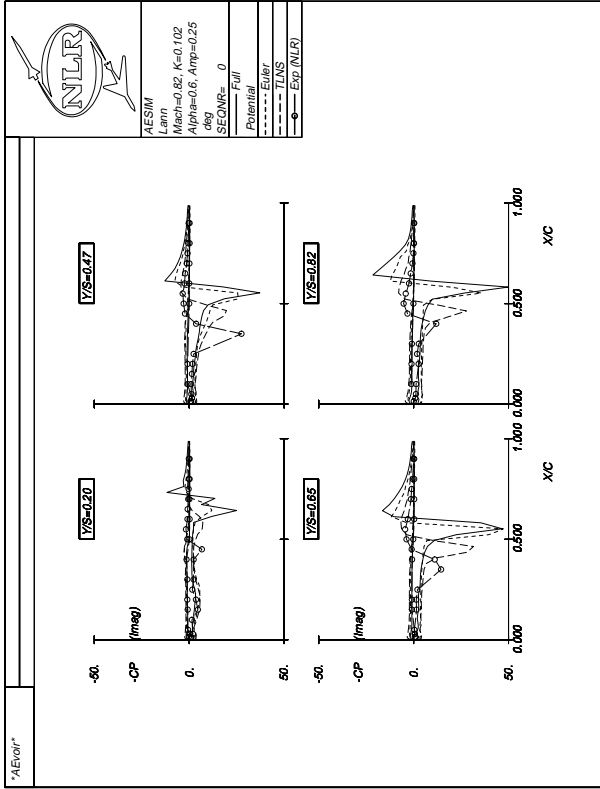


Figure 28: Comparison of imag. part of experimental with FP, EE and TLNS calculated first-harmonic pressure coefficients on LANN wing at $M_\infty = 0.82$, $\alpha_m = 0.6$ deg, $\alpha_{amp} = 0.25$ deg and $k = 0.102$.

application discussed in [8], will be reconsidered, viz. the 2-D AGARD standard test case for transonic viscous flow (case 3 of Landon [29]). The flow conditions are $M_\infty = 0.60$, $\alpha_m = 4.86$ deg, $Re_\infty = 4.8 \times 10^6$ and the boundary layer is fully turbulent. The mode of vibration is a pitching oscillation of the NACA 0012 profile about quarter-chord with an amplitude of 2.44 deg and a reduced frequency $k = 0.081$ based on semi-chord. In [8] the computational efficiency of the code for the current case was demonstrated for several variations of the iteration parameters, i.e. time steps/period, subiterations and Jacobian recalculations, thereby applying 2nd order extrapolation.

Comparison of calculated sectional coefficients, C_l and C_m (Fig. 29) for variety of time step simulations reveals that larger time steps/period for 3rd order extrapolation could be obtained, thereby reducing the computational cost, while maintaining adequate accuracy. Four cases of calculated results have been presented for high (400) to very low number (16) of time steps/period in combination with 4 and 12 subiterations, respectively. The lift coefficient shows a very good agreement. The moment coefficient shows a more sensitive behavior. Some differences are apparent, but the extremities appear to be captured well enough by all the cases. For this particular viscous test case it seems that 16 time steps with 12 subiterations is sufficient.

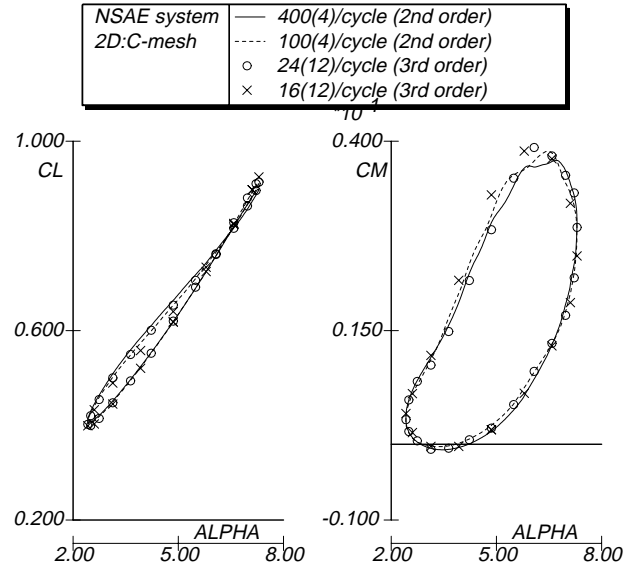


Figure 29: Comparison of sectional coefficients, C_l and C_m for variety of time step simulations, during oscillatory pitching motion of NACA 0012 profile at $M_\infty = 0.60$, $\alpha_m = 4.86$ deg, $Re_\infty = 4.8 \times 10^6$, $\alpha_{amp} = 2.44$ deg and $k = 0.081$.

4.2.4 Extrapolation methods in CAS

Driven by the requirement of realistic aeroelastic simulations, special attention is devoted not only to a proper modeling of the physics but also to their efficiency and robustness. Consequently, an important practical aspect is the capability to march accurately at a large time step, thereby reducing the overall turn-around time. However, this implies that all components of the simulation methodology should possess a **large time step** capability.

Therefore, an improvement of the aero-structural coupling procedures is necessary to benefit from the large time step allowed by the current aerodynamic methods, shown earlier. In [10] two coupling methods have been studied: an improved aerodynamic extrapolation method and a structural extrapolation method. Also a third one is introduced: the prognostic method. The latter is an extension of the structural extrapolation method and uses results of the time analysis to guess the new states. The three coupling approaches have been presented in detail in [10], therefore the main features will be discussed briefly and exemplified with a few applications.

In general the equations of motion for the aeroelastic system can be written into a standard state-space form as:

$$\dot{X} = AX + BU \quad (1)$$

A standard method [10] can be used to solve Eq.1:

$$\begin{aligned} X^{n+1} &= \Phi X^0 + \int_0^{t(n+1)} \Phi(t-\tau)BU(\tau)d\tau \\ &\approx \Phi(\Delta t)X^n + \Theta(\Delta t)\bar{U}, \end{aligned} \quad (2)$$

where \bar{U} is a representative value of the aerodynamic force $U(t)$ between time levels (n) and ($n+1$). Calculations

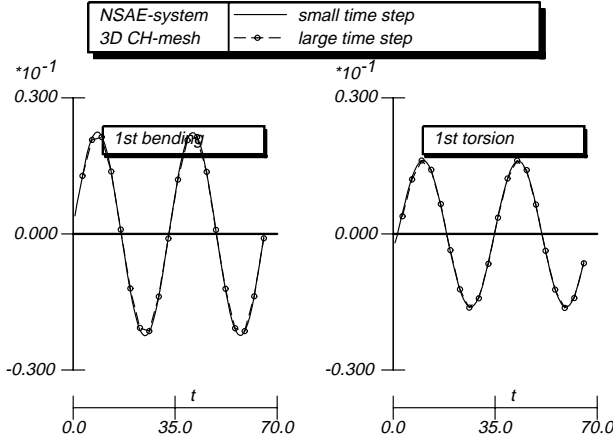


Figure 30: Comparison of time responses between small (48/period) and large (10/period) time step simulations for improved aerodynamic extrapolation method, for AGARD I-wing 445.6 at $M_\infty = 0.96$, $\alpha_m = 0.0$ deg, $amp = 0.005$ (2nd mode) and $k = 0.10$, during forced vibration.

lation of Φ and Θ are described in [10]. This commonly used loosely coupled method was originally suggested in [30], where the aerodynamic force $U(t)$ is assumed to vary linearly between time steps (n) and ($n+1$). The aerodynamic force at time level ($n + \frac{1}{2}$) is then extrapolated as:

$$U^{n+\frac{1}{2}} \approx \frac{3}{2}U^n - \frac{1}{2}U^{n-1}. \quad (3)$$

This value is used to represent the value of U between time step (n) and ($n+1$). This method fails, however, to give good results for large time steps simulations. Two approaches are studied to improve the method:

Aerodynamic extrapolation

The aerodynamic force is expressed as: $U = U(Q, X)$ and the extrapolation to time level ($n + \frac{1}{2}$) is:

$$U^{n+\frac{1}{2}} \approx U^n + \left(\frac{\partial U}{\partial Q} \frac{\partial Q}{\partial t} + \frac{\partial U}{\partial X} \frac{\partial X}{\partial t} \right) \frac{\Delta t}{2}. \quad (4)$$

where Q is defined by the TLNS equations [10]. The $\partial Q/\partial t$ and $\partial X/\partial t$ are readily available data while $\partial U/\partial Q$ and $\partial U/\partial X$ have to be calculated.

Structural extrapolation

The reason for this method is the fact that the structural part behaves smoother than the aerodynamic forces. Thus a better result may be expected from extrapolating the structural state. To obtain the aerodynamic force at time level ($n + \frac{1}{2}$), the state of the mesh is first approximated as:

$$X^{n+\frac{1}{2}} \approx X^n + \dot{X}^n \frac{\Delta t}{2}. \quad (5)$$

The \dot{x} in the second term is readily available while the \ddot{x} is approximated simply as $(\dot{x}^n - \dot{x}^{n-1})/\Delta t$. Using this data a mesh is generated and the surface velocity is used to enforce the boundary condition.

Thus the aerodynamic part of the method marches at a time level between the structural states. This method is more efficient than the first one since all quantities needed for extrapolation are readily available or can be easily calculated.

To show the applicability of the improved extrapolation methods for large time step simulations a forced vibration case [10] of the 3-D configuration for dynamic response I-wing 445.6 model *weakened no.3* is presented. Only calculation results with EE are shown. The applied grid consists of $121 \times 29 \times 24$ mesh points. The case at $M_\infty = 0.96$ is considered. The second mode of the wing is excited in a sinusoidal motion with reduced frequency $k = 0.10$, based on root semi-chord, and an amplitude of 0.005. Figure 30 shows the response of the first two vibration modes using a small time step (48 steps/period) and a large time step (10 steps/period). The conclusion is that no significant differences are observed. Other applications have been demonstrated in [10].

Finally a prognostic method is proposed, which is discussed in the next section.

4.2.5 Prognostics using TAM in CAS

The prognostic method proposed in [10] which is a refinement/generalization of the previous extrapolation methods and might be regarded as a higher-order extrapolation using transfer functions. In each time step the structural or aerodynamic part is extrapolated to the next time level by:

$$X^{(n+\frac{1}{2})} \approx P \left(X, U, n + \frac{1}{2} \right) \text{ or}$$

$$U^{(n+\frac{1}{2})} \approx P \left(X, U, n + \frac{1}{2} \right)$$

Here $P(\#, t)$ denotes the approximation of time trace $\{\#_n, \#_{n-1}, \dots, \#_{n-m}\}$ at t which should be obtained by performing one of time analysis methods (TAM) presented in [10], m denotes the number of retarded time steps in the time domain. It will be obvious that as soon as the function P is not changing anymore the simulation can be finished since the following time steps will not present any new additional information. In fact this means the time step is virtually infinite.

A 2-D aeroelastic application of the prognostic extrapolation method, discussed in [10], is presented for the NACA 64A010 airfoil using structural data from the Isogai case A [31]. The structural parameters are $a=-2.00$, $x_\alpha=1.80$, $r_\alpha^2=3.48$, $\mu=60.00$ and the ratio of the uncoupled frequency $\omega_h/\omega_\alpha=1.00$. The flutter boundaries of this case, compared to some other methods, have already been shown in [8]. The result presented here will concentrate on the large time step aspect of the method. A mesh consisting of 140×32 points was applied. Only application with EE equations will be presented. The simulation is started from a steady condition with an initial \dot{x} . The small time step simulation uses 32 time steps/period of the uncoupled mode while the large time step simulation applies 8 time steps/period.

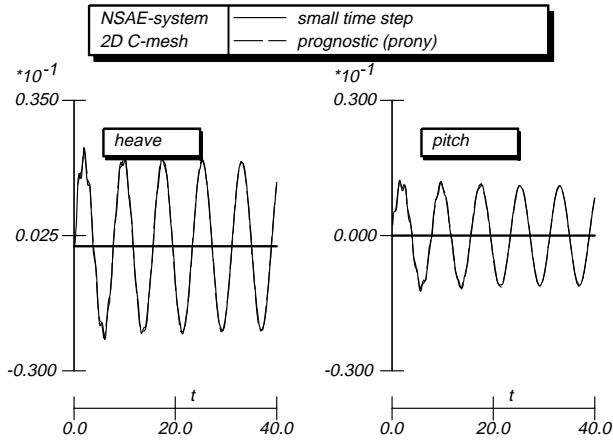


Figure 31: Comparison of time responses between small (32/period) and large (8/period) time step simulations for the prognostic method, employing Prony's method, on Isogai case A at $M_\infty = 0.85$.

The case considered is a subcritical condition at $M_\infty = 0.85$ with $V^* = U_\infty / (\omega_\alpha b \sqrt{\mu}) = 0.53$. Comparison of simulation using small time steps and large time steps for the prognostic method, employing Prony's [11] analysis for the time traces is shown in figure 31. The results of both simulations show an excellent agreement, no differences are observed. The inadequacy of the common method [30] for large time step simulations of this case have been shown in [10].

4.3 Linear Aero Research

To ease applications and to build confidence a coupled aeroelastic simulation should also be run based on linear aerodynamics. This requires the generalized aerodynamic forces (transfer functions) which are in general available in the frequency domain to be fitted [23, 32] and transformed to the time-domain.

Figure 32 shows a number of possibilities to calculate the generalized aerodynamic forces together with the transformation tools to obtain transfer function repre-

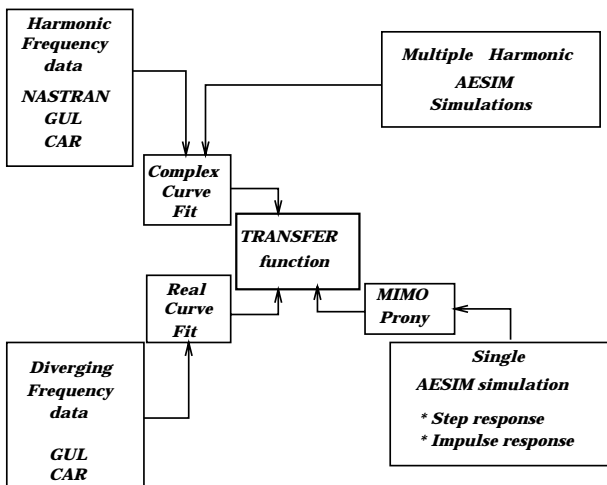


Figure 32: Flowchart of techniques for transforming linear aerodynamics between frequency and time domain.

sentations of the loads for ease formulation in the time domain. The blocks in the four outer corners of the diagram are sources to calculate the aerodynamic forces. The three inner blocks around the kernel of the diagram, **transfer function**, are fitting procedures for the aerodynamic forces. These fitting procedures include: 1) Complex curve fit in **s**-domain, 2) Real fit curve in **s**-domain, and 3) MIMO-class techniques and Prony's method, which have been described in [11].

A feasibility study with 2-D airloads and 3-D airloads has been performed [11] to investigate the most efficient way to embed linear aerodynamics in the AESIM method. Without the analytical details the procedure was as follows [11].

The assumption is made that the behavior of any unsteady parameter of interest such as an aerodynamic load or a pressure coefficient can be described by an appropriate form for the transfer function which is a ratio of two **s** dependent polynomials which is known as the Padé approximation. The complex fitting procedure has been assumed to obtain the approximation. The rational polynomial has been transformed to the state-space form. Subsequently, this system has been solved using the Newmark scheme embedded in the AESIM system. Two applications of the study will be presented, a 2-D case for a flat plate and a 3-D case of the AGARD I-wing 445.6.

2-D application Calculations of unsteady airloads have been performed with DOULAT for a flat plate heaving (mode 1) and pitching about an axis $0.5c$ in front of the leading edge (mode 2) at $M_\infty = 0.5$ and a reduced frequency range up to $|s| = 1.0$. (Note: The reduced frequency is defined here as $k = Im(s)$, based on the semi-chord.) The generalized forces data generated by DOULAT were fitted with the afore-mentioned procedure. Thereafter the Newmark scheme was applied to oscillatory motions in the same frequency range and the time traces were transformed to the frequency domain.

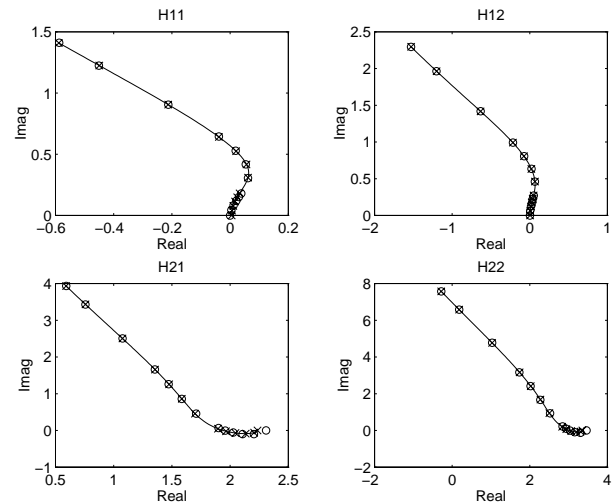


Figure 33: Comparison of directly calculated and fitted unsteady coefficients of a harmonically heaving and pitching flat plate at $M_\infty = 0.5$.

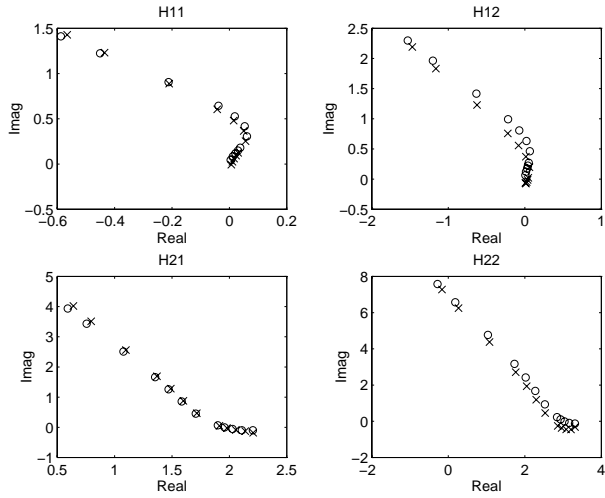


Figure 34: Comparison in the frequency domain of directly calculated and to and fro transformed unsteady coefficients of a harmonically heaving and pitching flat plate at $M_\infty = 0.5$.

Figure 33 shows the comparison in the frequency domain between the original data (circle) and the fitted data (line-cross) which show a good agreement. Figure 34 shows the comparison in the frequency domain between the original data (circle) and the data (cross) obtained by analysing the time traces which again show a good agreement. From this the conclusion might be drawn that the aforementioned procedure is applicable in 2-D.

3-D application Calculations have also been performed with GUL for the 3-D AGARD I-wing 445.6 at $M_\infty = 0.901$. This configuration is described in [26]. Again two modes were selected, modes 2 and 4. A similar procedure was applied as outlined above. Figure 35 shows the comparison in the frequency domain between the original data (circle) and the fitted data (line-cross) which show a good agreement. Figure 36 shows a comparison in the frequency domain between the original data (circle) and the data (cross) obtained by analysing the time traces which shows again a good agreement.

From this the conclusion might be drawn that the aforementioned procedure shows good promise for embedding in the AESIM system.

4.4 LCO simulation system

Modern fighter-type aircraft operating in the high subsonic, transonic and low supersonic speed regime may experience under certain conditions transonic nonlinear flutter, known as limit cycle oscillations (LCO). The phenomenon is related to flutter but affects aircraft performance in a manner similar to buffet. Conditions of transonic LCO instabilities are moderate angle-of-attack, usually smaller than 10 deg and transonic Mach numbers ranging from ~ 0.9 to ~ 1.1 . The flow conditions during this type of LCO are characterized by **mixed attached/separated flow**. Lowly damped vibration modes tend to respond provided they have the

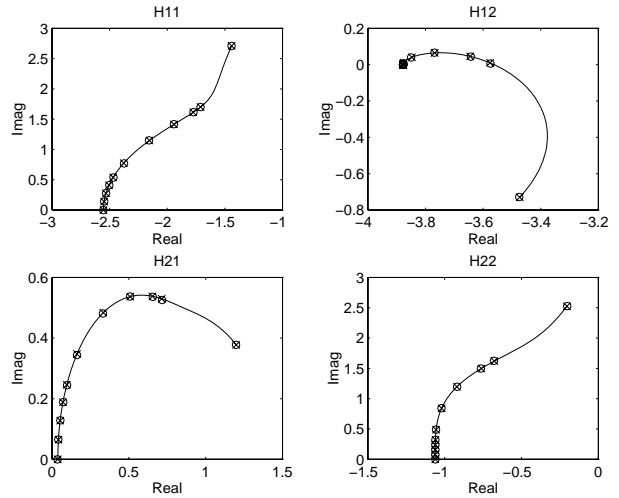


Figure 35: Comparison of directly calculated and fitted unsteady coefficients of the harmonically oscillating AGARD I-wing 445.6 at $M_\infty = 0.901$, (modes 2 and 4).

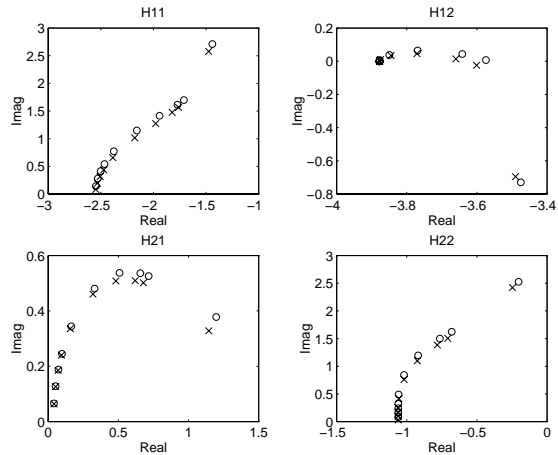


Figure 36: Comparison in the frequency domain of directly calculated and to and fro transformed unsteady coefficients of the harmonically oscillating AGARD I-wing 445.6 at $M_\infty = 0.901$, (modes 2 and 4).

proper characteristics to couple with this type of flow. The coupling frequently occurs near flutter boundaries obtained with linear theory [14], i.e. with panel methods for attached flow.

To determine accurately this kind of nonlinear aeroelastic instabilities, an investigation was started at NLR in the early nineties to understand the nature of LCO experienced by fighter-type aircraft maneuvering at transonic speeds. In addition to conducting an extensive wind tunnel investigation on oscillating fighter type wings [3, 20, 33], a major objective was to develop a semi-empirical method for predicting LCO [12, 13, 15] characteristics of full scale aircraft.

As part of the method, a model for determining aerodynamic loads from steady and unsteady data bases was developed that is suitable for predicting LCO of fighter-type aircraft at transonic speeds. Based on previous

studies using steady pressure data [33], it was shown that time lags in the aerodynamic flow field are essential to obtain realistic LCO amplitudes. Analysis of unsteady wind tunnel data obtained from [3, 20] showed that these aerodynamic time lags are affected by the various types of flow field involved. Further, on the basis of the knowledge of these flow field types and the results of the unsteady wind tunnel measurements, an aerodynamic (pressure) state-space model was developed by NLR, for transforming the unsteady highly nonlinear aerodynamic loads into a form appropriate for use in time simulation methods. This pressure model is similar to the nonlinear “ONERA” aerodynamic model initially developed by Tran & Petot [34]. The development of the NLR unsteady pressure model and capability of producing nonlinear transonic aerodynamics that are typical of transonic LCO were presented in [12, 13, 15]. It was also demonstrated for a number of aircraft configurations [12, 13, 15] that the current status of the semi-empirical LCO prediction method with implementation of the NLR unsteady pressure model produced results which correlate correctly with flight test data.

The above description of the NLR pressure model shows that extensive use is made of steady and unsteady wind tunnel test data. It is clear that the effectiveness and reliability of the model strongly depends on the completeness of the experimental data base and the thoroughness of the evaluation of the model. These, however, have been obtained on a limited scale in the present research program. Continued research is therefore needed to enhance the confidence in the model and to establish its applicability for wide ranges of model and flow parameters. Such research may be defined in one or more of the following directions.

- Continued pressure and load measurements in the wind tunnel.

The aim of this test is to extend the unsteady part of the data base, which currently corresponds to a limited number of model and flow parameter values, and so to bring it in balance with the steady part [33] of the data base, which corresponds to an extensive set of parameter values. Particularly, interest exists in collecting data for more leading-edge and trailing-edge flap deflections and denser frequency ranges (e.g. frequency sweeps). In the test use can be made of the existing wind tunnel model.

- Application of CUA/CAS.

CUA For model configurations and flow conditions which have not or can not be represented in a wind tunnel test program the required aerodynamic information may be obtained from CUA-techniques, steady and unsteady. The current development of these techniques shows that they are very promising, even for the complicated types of flow including flow separation (see sections 3 and 4), but that they have matured more sufficiently.

It is to be expected that in the near future these CUA-techniques may play a complementary role. Measured steady and unsteady pressure and loads data [3, 20, 33] may be used to validate those techniques.

CAS Extensions for typical fighter-type aircraft applications of the discussed **AESIM** system to perform realistic computational aeroelastic simulations. Because of the modular design of the system, such extensions should be carried out relative easy. Measured flight test data may be used to validate the updated **AESIM** system. Further, calculated aeroelastic responses may be compared with results of the semi-empirical prediction method, or vice-versa.

Realization of the suggested extension of the **AESIM** system will enhance the aeroelastic analysis capability for fighter-type aircraft as depicted in figure 37.

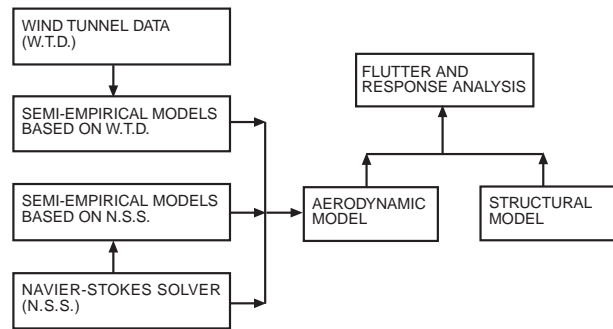


Figure 37: Classification of prediction methods.

Aero-elastic Simulation Method

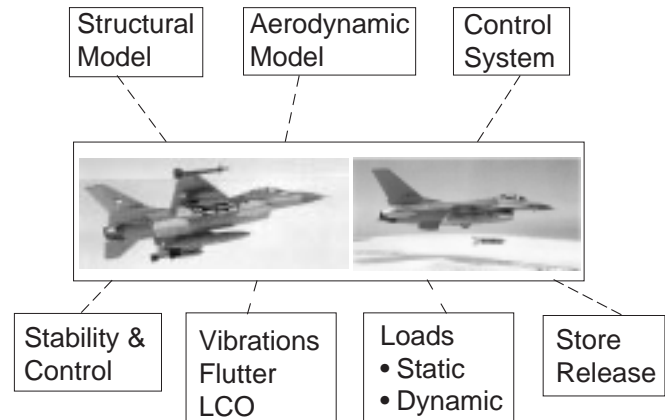


Figure 38: Future developments of AEroelastic SIMulation method.

5. FUTURE RESEARCH ACTIVITIES

Future aeroelastic research activities will be focused on realistic and affordable aeroelastic simulations depicted in figure 38. The aim is to extend the current **AESIM**

system to an aeroelastic simulation environment for fighter-type aircraft application.

Starting with the basic ingredients of the aircraft:

- Structural modelling,
- Aerodynamic modelling and
- Control system modelling,

the following analyses have to be performed in more or less detail:

- Vibrations in general, flutter and non-linear flutter (LCO),
- Loads: static and dynamic, including deformations,
- Aeroelastic responses due to store release and
- Impact of control system on aeroelastic responses.

6. CONCLUSIONS

In this paper the status of the NLR system for aeroelastic simulations has been presented and demonstrated with an up to date account of applicability. Experiences with recent applications and ongoing developments led to the following observations:

- Given the accuracy of the aerodynamic modelling the most critical part in the Aeroelastic SIMulation is the geometry handling.
- The interpolation at the fluid/structure interface can be carried out satisfactorily with the available models.
- The volume spline method has proven its value as interpolation tool for structured as well as unstructured data.
- The analysis of time-signals can be carried out satisfactorily with the available models.
- The availability of direct graphical monitoring of all relevant data is crucial.
- The effort to obtain consistency between the geometrical and elastomechanical input data sets is often overlooked in interdisciplinary use.
- Sufficiently accurate results: EE/TLNS at 8/48 time steps per period.
- Adequate coupled EE results are obtained using 8 time steps per cycle.
- Present 3D EE/TLNS aerodynamic computations are about 5/15 times slower compared to FP.
- Recent applications show increased affordability.

ACKNOWLEDGEMENT

This investigation has partly been carried out under contract with the Netherlands Agency for Aerospace Programmes (NIVR), contracts 01904N and 07801N, and partly under contract with the Royal Netherlands Air Force (RNLAf). The LCO investigation was also funded by U.S. Air Force and Lockheed Martin Tactical Aircraft Systems (LMTAS), Fort Worth, Texas, contract F33657-84-C-0247 (CCP 4551).

REFERENCES

- 1 Hounjet, M.H.L., "NLR Inviscid Transonic Unsteady Loads Prediction Methods in Aeroelasticity", AGARD SMP Specialist Meeting on Transonic Unsteady Aerodynamics and Aeroelasticity, San Diego, California, 9-11 October 1991, AGARD CP 507.
- 2 Meijer, J.J., Cunningham, Jr., A.M., "Development of a Method to Predict Transonic Limit Cycle Oscillation Characteristics of Fighter Aircraft", AGARD SMP Specialist Meeting on Transonic Unsteady Aerodynamics and Aeroelasticity, San Diego, California, 9-11 October 1991, AGARD CP 507.
- 3 Cunningham, Jr., A.M., Boer, R.G. den, "Transonic Wind Tunnel Investigation of Limit Cycle Oscillations on Fighter Type Wings", AGARD SMP Specialist Meeting on Transonic Unsteady Aerodynamics and Aeroelasticity, San Diego, California, 9-11 October 1991, AGARD CP 507.
- 4 Burt, M., "The Impact of Computational Unsteady Aerodynamics in Aerospace Engineering – Past, Present and Future", European Forum: Recent Developments and Applications in Aeronautical CFD, 1-3 September 1993, Bristol, UK (paper 12).
- 5 Hounjet, M.H.L., and Eussen, B.J.G., "Outline and Application of the NLR Aeroelastic Simulation Method", 19th ICAS Congress, Anaheim, California, September 18-23, 1994.
- 6 Eussen, B.J.G., Hounjet, M.H.L., Zwaan, R.J., "Experiences in Aeroelastic Simulation Practices", Euromech-colloquium 349: Simulation of fluid-structure interaction in aeronautics, Göttingen, Germany, September 16-18, 1996.
- 7 Hounjet, M.H.L., Meijer, J.J. "Evaluation of Elastomechanical and Aerodynamic Data Transfer Methods for Non-Planar Configurations in Computational Aeroelastic Analysis", International Forum on Aeroelasticity and Structural Dynamics 1995, Manchester, UK, 26-28 June 1995.
- 8 Prananta, B., Hounjet, M.H.L., Zwaan, R.J., "A Thin Layer Navier-Stokes Solver and its Application for Aeroelastic Analysis of an Airfoil in Transonic Flow", International Forum on Aeroelasticity and Structural Dynamics 1995, Manchester, UK, 26-28 June 1995.
- 9 Prananta, B.B., Hounjet, M.H.L., "Aeroelastic Simulation with Advanced CFD Methods in 2-D and 3-D Transonic Flow", Symposium Unsteady Aerodynamics 1996, RAeS, London, UK, July 17-18, 1996.
- 10 Prananta, B.B., Hounjet, M.H.L., "Large Time Step Aero-Structural Coupling Procedures for Aeroelastic Simulation", International Forum on Aeroelasticity and Structural Dynamics, Rome, Italy, 17-20 June 1997.

- 11 Hounjet, M.H.L., Eussen, B.J.G., Soijer, M.W., "Analysis of Computational Aeroelastic Simulations by Fitting Time Signals", International Forum on Aeroelasticity and Structural Dynamics, Rome, Italy, 17-20 June 1997.
- 12 Meijer, J.J., Cunningham, Jr., A.M., "Outline and Applications of a Semi-Empirical Method for Predicting Transonic Limit Cycle Oscillation Characteristics of Fighter Aircraft", International Forum on Aeroelasticity and Structural Dynamics 1995, Manchester, UK, June 26-28, 1995.
- 13 Meijer, J.J., "Modeling of Semi-Empirical Transonic Unsteady Aerodynamics for Predicting Limit Cycle Oscillation Characteristics of Fighter Aircraft", 20th ICAS Congress, Sorrento, Italy, September 8-13, 1996.
- 14 Meijer, J.J., Hounjet, M.H.L., "Evaluation of Aeroelastic Methods to Predict Wing/Store Flutter at Subsonic, Transonic and Supersonic Speeds", Euromech-colloquium 349: Simulation of fluid-structure interaction in aeronautics, Göttingen, Germany, September 10-12, 1996.
- 15 Meijer, J.J., "Determination of Transonic Unsteady Aerodynamic Loads to Predict the Aeroelastic Stability of Fighter Aircraft", International Forum on Aeroelasticity and Structural Dynamics 1997, Rome, Italy, June 17-20, 1997.
- 16 Hounjet, M.H.L., "Hyperbolic grid generation control by panel methods", NLR TP 91061 U, June 1991.
- 17 Chan, W.M. and Steger, J.L., "A generalised scheme for three-dimensional hyperbolic grid generation", AIAA-91-1588-CP, July 1991.
- 18 Hounjet, M.H.L. and Eussen, B.J.G., "AESIM: An Aeroelastic simulation method for transport aircraft in transonic flow", NLR CR 96009 C, January 1996
- 19 Westland, J., and Hounjet, M.H.L., "Clebsch variable model for unsteady, inviscid, transonic flow with strong shock waves", AIAA 93-3025, July 1993.
- 20 Cunningham, Jr., A.M., Boer, R.G. den, "Transonic Wind Tunnel Investigation of Limit Cycle Oscillations on Fighter Type Wings – Update", 33rd AIAA, ASME, ASCE, AHS, ASC, SDM Conference, Dallas, Texas, April 13-17, 1992.
- 21 Soijer, M.W., "Frequency Domain Identification of Rotorcraft State Space Models and Applications to a BO105 Rigid Body Model", Master's thesis, Delft University of Technology, Faculty of Aerospace Engineering, December 1996
- 22 Hounjet, M.H.L., "Calculation of unsteady subsonic and supersonic flow about oscillating wings and bodies by new panel methods", NLR TP89119 U, April 1989.
- 23 Hounjet, M.H.L., Eussen, B.J.G. "Prospects of time-linearized Unsteady Calculation Methods for Exponentially Diverging Motions in Aeroelasticity", 33rd AIAA, ASME, ASCE, AHS, ASC, SDM Conference/Dyn. Spec. Conference, Dallas, Texas, April 13-17, 1992.
- 24 Yates, C., "AGARD Standard Aeroelastic Configurations for Dynamic Response I-Wing 445.6", AGARD Report No. 765, 1988.
- 25 Cunningham, Jr., A.M., den Boer, R.G., Dogger, C.S.G., Geurts, E.G.M., Retèl, A.P., Zwaan, R.J. "Unsteady Transonic Wind Tunnel Test on a Semi-Span Straked Delta Wing Model Oscillating in Pitch", NLR CR 93570 L (parts I through III) 1993.
- 26 Bland, S.R., "AGARD Three dimensional aeroelastic configurations", AGARD Report AR-167, June 1979.
- 27 AGARD, "Compendium of unsteady aerodynamic measurements", AGARD Report R-702, Neuilly-sur-Seine, August 1982.
- 28 Hounjet, M.L.H., Meijer, J.J., "Application of Time-Linearized Methods to Oscillating Wings in Transonic Flow and Flutter", AGARD CP-374, September 1984.
- 29 Landon, R., "NACA 0012 oscillatory and transient pitching", Compendium of unsteady aerodynamic measurements", AGARD Report R-702, Neuilly-sur-Seine, August 1982.
- 30 Edwards, J.W., Bennett, R.M., Whitlow, Jr., W., Seidel, D.A., "Time-marching Transonic Flutter Solutions including Angle-of-attack Effects", J. Aircraft, Vol.20, No.11, Nov.1983, pp. 899-906.
- 31 Isogai, K., "On the transonic dip mechanism of flutter of sweptback wing", AIAA Journal vol.7, July 1979, pp 793-795.
- 32 Hounjet, M.H.L., Eussen, B.J.G., "Beyond the Frequency Limits of Time-Linearized Methods", International Forum on Aeroelasticity and Structural Dynamics, Aachen, Germany, June 1991.
- 33 Elbers, W.K., "Wind Tunnel Data Report 1/9-Scale F-16A Pressure Model Investigation of Shock-Induced Separation for Limit Cycle Oscillation Studies (AEDC PWT-16T Test TF-695)", General Dynamics, Fort Worth Division Report 16PR4694, September 1985, (Contract No. F33657-84-C-2034).
- 34 Tran, C.T., Petot, D., "Semi-Empirical Model for the Dynamic Stall of Airfoils in View of the Application to the Calculation of Responses of a Helicopter Blade in Forward Flight", Vertica, Vol.5, 1981.